Multi-Method Approach to the Early Postnatal Growth of the Mandible in Mice from a Zone of Robertsonian Polymorphism

JESSICA MARTÍNEZ-VARGAS[1,*], FRANCESC MUÑOZ-MUÑOZ[1], MARÍA JOSÉ LÓPEZ-FUSTER[2], JORGE CUBO[3], and JACINT VENTURA[1]

[1]Departament de Biologia Animal, de Biologia Vegetal i d'Ecologia, Facultat de Biociències, Universitat Autònoma de Barcelona, E-08193 Bellaterra (Cerdanyola del Vallès), Spain

[2]Departament de Biologia Evolutiva, Ecologia i Ciències Ambientals, and Institut de Recerca de la Biodiversitat (IRBio), Facultat de Biologia, Universitat de Barcelona, Av. Diagonal 645, E-08028 Barcelona, Spain

[3]Sorbonne Universités, UPMC Univ Paris 06, Institut des Sciences de la Terre Paris (iSTeP), 4 place Jussieu, BC 19, F-75005 Paris, France

Running title: POSTNATAL MANDIBLE GROWTH IN WILD HOUSE MICE.

Grant sponsors: Spanish Ministry of Economy and Competitiveness, and Government of Catalonia; Grant numbers: CGL2010-15243, and 2014-SGR-1241.

* Correspondence to: Jessica Martínez-Vargas; Departament de Biologia Animal, de Biologia Vegetal i d'Ecologia; Facultat de Biociències; Avinguda de l'Eix Central, Edifici C; Campus de la UAB; Universitat Autònoma de Barcelona; E-08193 Bellaterra (Cerdanyola del Vallès); Spain.
Phones: (+34)638323651, (+34)935813744. Fax: (+34)935811321.
E-mails: jessmv88@gmail.com, Jessica.Martinez.Vargas@uab.cat.

ABSTRACT

The western European house mouse (*Mus musculus domesticus*) shows high karyotypic diversity owing to Robertsonian translocations. Morphometric studies conducted with adult mice suggest that karyotype evolution due to these chromosomal reorganizations entails variation in the form and the patterns of morphological covariation of the mandible. However, information is much scarcer regarding the effect of these rearrangements on the growth pattern of the mouse mandible over early postnatal ontogeny. Here we compare mandible growth from the second to the eighth week of postnatal life between two ontogenetic series of mice from wild populations, with the standard karyotype and with Robertsonian translocations respectively, reared under the same conditions. A multi-method approach is used, including bone histology analyses from mandible surfaces and cross-sections, as well as geometric morphometric analyses of mandible form. The mandibles of both standard and Robertsonian mice display growth acceleration around weaning, anteroposterior direction of bone maturation, a predominance of bone deposition fields over ontogeny, and relatively greater expansion of the posterior mandible region correlated with the ontogenetic increase in mandible size. Nevertheless, differences exist between the two mouse groups regarding the timing of histological maturation of the mandible, the localization of certain bone remodeling fields, the temporospatial patterns of morphological variation, and the organization into two main modules. The dissimilarities in the process of mandible growth between the two groups of mice become more evident around sexual maturity, and could arise from alterations that Robertsonian translocations may exert on genes involved in the bone remodeling mechanism.

Key words: bone histology; bone remodeling; geometric morphometrics; *Mus musculus domesticus*; Robertsonian translocations

INTRODUCTION

The western European house mouse, *Mus musculus domesticus* Schwarz and Schwarz, 1943, has a standard (St) karyotype of 40 acrocentric chromosomes (2n=40), but shows high variability in chromosome number due to Robertsonian (Rb) translocations (Piálek et al., 2005). These are spontaneous chromosomal rearrangements that consist in the centromeric fusion of the long arms of two non-homologous acrocentric chromosomes, resulting in the formation of metacentric chromosomes and, thus, in the decrease in diploid number (Gropp and Winking, 1981). Because of its high karyotypic diversity, *M. musculus domesticus* is a widely used model organism for the study of evolutionary processes linked to chromosomal reorganizations, such as reproductive isolation and phenotypic variation (Piálek et al., 2005; Chmátal et al., 2014; Franchini et al., 2016).

The Rb systems are defined as ensembles of populations from restricted geographical areas that share a set of metacentrics, resulting from Rb translocations, with a common evolutionary origin (Capanna et al., 1974; Piálek et al., 2005). In this scenario, Rb populations are surrounded by populations formed by specimens with the St karyotype. Within the distribution area of *M. musculus domesticus*, many Rb systems with different sets of metacentrics have been formally recognized (for reviews, see Piálek et al., 2005; Gündüz et al., 2010; Hauffe et al., 2012; Garagna et al., 2014). The 'Barcelona' Rb system, located in Northeastern Iberian Peninsula, is characterized by seven different metacentrics (Rb(3.8), Rb(4.14), Rb(5.15), Rb(6.10), Rb(7.17), Rb(9.11), Rb(12.13)) with a staggered distribution over 5,000km^2, a high level of chromosomal polymorphism, and the absence of a metacentric race (*sensu* Hausser et al., 1994; see Adolph and Klein, 1981; Gündüz et al., 2001; Sans-Fuentes et al., 2007; Medarde et al., 2012). The broad study of this Rb system has highlighted that Rb translocations can influence several biological processes and patterns, such as spermatogenesis and sperm form (Sans-Fuentes et al., 2010; Medarde et al., 2013, 2015), genetic recombination (Capilla et al., 2014), and morphological variation (Muñoz-Muñoz et al., 2003, 2006, 2011; Sans-Fuentes et al., 2009; Martínez-Vargas et al., 2014).

The mandible of the house mouse is a primary model system for evo-devo, genetic, morphological, and functional studies of complex morphological structures, as well as for research addressing the

effect of Rb translocations on phenotypic traits (Atchley and Hall, 1991; Corti and Rohlf, 2001; Klingenberg et al., 2004; Muñoz-Muñoz et al., 2011; Klingenberg and Navarro, 2012; Martínez-Vargas et al., 2014). This bony structure has also been the focus, on numerous occasions, of analyses of morphological modularity and integration, which have traditionally recognized the existence of two main developmental and functional modules: the alveolar region (or mandibular corpus), which bears the teeth, and the ascending ramus, where most of the masticatory muscles attach to (Atchley and Hall, 1991; Cheverud et al., 1997; Ehrich et al., 2003; Klingenberg et al., 2003; Muñoz-Muñoz et al., 2011; Fruciano et al., 2013). The mouse mandible, like the rest of bones, attains its adult form (i.e., size and shape) over postnatal life through bone growth remodeling (*sensu* Enlow 1963, 1982 – however, discrepancy exists in the terminology used to refer to this growth process depending on the field of bone research; for further discussion see Martinez-Maza et al., 2006, 2010). This mechanism involves the coordinated, uncoupled and ongoing cellular activity of osteoblasts and osteoclasts, which respectively carry out bone deposition and bone resorption (Bloom and Fawcett, 1994; Enlow and Hans, 1996). Although the activities of these bone cells are genetically controlled, they may also be influenced by endogenous and exogenous factors (Robling et al., 2006; Burr and Allen, 2013). Since the functions of osteoblasts and osteoclasts leave different peculiar histological microfeatures on bone surfaces, it is feasible to characterize the spatial distribution of bone deposition and resorption fields using bone surface histology. The resulting cell activity maps are known as bone remodeling patterns (Bromage, 1989; Enlow and Hans, 1996; Martinez-Maza et al., 2010). Furthermore, the bone remodeling mechanism can be analyzed from histological cross-sections after the *in vivo* supply of vital fluorescent dyes that adhere to the mineralization front of the growing bone tissue (Pautke et al., 2005; van Gaalen et al., 2010). Moreover, the speed of bone deposition determines the internal microstructure of bones, whose histological analysis can thus also provide clues about the growth pattern: fast bone deposition results in woven bone tissue, while parallel-fibered and especially lamellar bone tissue are associated with slower bone deposition (Amprino, 1947; de Buffrénil and Pascal, 1984; Castanet et al., 2000; Currey, 2002; de Margerie et al., 2004).

Several studies have revealed variation in the form and the patterns of morphological covariation of the mouse mandible, as well as difference in its level of modularity, linked to the presence and/or

amount of Rb translocations (e.g., Corti and Rohlf, 2001; Muñoz-Muñoz et al., 2011; Fruciano et al., 2013; Martínez-Vargas et al., 2014; Franchini et al., 2016). Nonetheless, these studies have been typically conducted with adult mice, while there is a shortage of information about the effect of Rb translocations on the growth and covariational properties of the mouse mandible during early postnatal ontogeny. Since the adult form of a morphological structure largely depends on its growth pattern over postnatal life, it would be reasonable to hypothesize that the early postnatal growth process of the mandible might also differ between mice with the St karyotype and mice with Rb translocations. Given that bone remodeling is responsible for postnatal bone growth, it could be also hypothesized that potential differences between mice with and without Rb translocations in the early postnatal patterns of mandible form variation might result from differences between their patterns of mandible remodeling. In addition, it could be suggested that differences in the level of modularity of the mandible between mice with the St karyotype and with Rb translocations might also be detected during early postnatal life.

In the present study, we examine and compare mandible growth and covariation from the 2nd to the 8th week of postnatal life between two ontogenetic series: mice with Rb translocations from the 'Barcelona' Rb system, and mice with the St karyotype from surrounding St populations. Our approach includes different methodologies: (1) analysis of internal microstructure, remodeling, and growth rates through the examination of fluorescent labels in histological cross-sections; (2) characterization of remodeling patterns with bone surface histology; and (3) analysis of form variation by means of geometric morphometrics. This comparative study intends to broaden the scarce knowledge of the growth process of the mouse mandible during early postnatal life while assessing the effect of a set of Rb translocations on phenotypic variation and covariation of this bony structure.

MATERIALS AND METHODS

Sample

Pregnant females of *M. musculus domesticus* were live-captured in the 'Barcelona' Rb system (n=11) and surrounding St populations (n=10) with Sherman traps between the years 2009 and 2014.

All females were transferred to an animal room at the Universitat Autònoma de Barcelona (Barcelona, Spain), with controlled conditions and a natural light cycle, and were separately housed in standard cages with environmental enrichment. They were supervised daily and the day of birth of each litter was noted. Water and standard rodent pellets were provided *ad libitum* in all cages.

The newborn mice were housed together with their biological mothers and were not manipulated during their first week of postnatal life, with the aim of ensuring their survival. The sample used in this study consisted of 79 individual mice that survived this critical period just after birth and remained alive until their stipulated date of euthanasia: 43 individuals born from the females trapped within the 'Barcelona' Rb system (hereafter cited as 'Rb mice'), and 36 individuals born from the females captured in surrounding St localities (hereafter cited as 'St mice') (Appendix 1). From their 7th day of postnatal life, each litter was housed in a cage with a breeding female of the C57BL/6J mouse strain and her biological offspring. Standard rodent pellets and water were always provided *ad libitum*. Own and adoptive offspring of each wet-nurse female were about the same age. When the final litter size of the foster mothers exceeded their average number (6-8 pups), some of their own pups were removed. The litters of these breeding females were not included in this study. Because wild mammals are more prone to suffer, and recover worse, from stress in captivity than domesticated mammals, the breeding performance of wild mammals can be more severely affected by stressful factors (Wallace, 1976). Given that female mice perform communal nursing (Manning et al., 1995; Hayes, 2000), the aforementioned fostering strategy was chosen to avoid that the stress experienced by the wild females under captive conditions could compromise the survival and growth of their pups, and to guarantee that all mice grew under similar conditions. All mice fed on milk from females with the same breeding performance until weaning, which in the house mouse occurs around the 21st postnatal day, and afterwards they were fed the same diet, consisting of rodent pellets.

Mice were allowed to grow until the end of the 2nd–8th postnatal week (hereafter 'PW'), and sample sizes were balanced among weeks, as much as possible, within the two mouse groups (Table 1 and Appendix 1). Specimens were euthanized by cervical dislocation, and their karyotypes were obtained from marrow cells of the femurs and dyed with Wright stain (Ford, 1966; Mandahl, 1992). Chromosomes were identified under a light microscope (Nikon Eclipse 50i) according to the

Committee on Standardized Genetic Nomenclature for Mice (1972). The diploid number, together with the specific set of metacentrics and their state of structural heterozygosity, were recorded for as many individuals as possible. As expected, Rb mice had metacentrics (2n=28–37), while St mice had the St karyotype (2n=40) (Appendix 1). The mandibles, or dentary bones, of all specimens were dissected, and their left and right sides were separated from each other at the mandibular symphysis and cleaned by hand as carefully as possible. The timing of tooth eruption as seen from the lingual mandible view was qualitatively examined in both ontogenetic series.

It should be noted here that the particular characteristics of the 'Barcelona' Rb system conditioned the composition of the sample and the experimental design of the present study. First, the high level of Rb polymorphism in the zone under study (see Medarde et al., 2012) led to the acquisition of individuals with multiple different combinations of Rb translocations. Due to the protocol followed, the karyotypes of the specimens could only be identified after euthanasia. Second, it was not feasible to separately test the effect of each different Rb translocation on mandible growth, since all Rb specimens included in this study always had more than two different metacentrics. Third, the difficulties in trapping evidently pregnant wild female mice, and in successfully breeding them and their pups under laboratory conditions, led to relatively small sample sizes in each postnatal week and group considered. The attempt to increase the sample sizes would have entailed lengthening the trapping over a considerably long time period, and even so, in the case of Rb mice it might have not been feasible to obtain individuals with specific karyotypes. These issues constitute the main limitations of the study; they explain the pooling of different Rb karyotypes in a single Rb group and therefore they account for the exploratory nature of the comparisons made between St and Rb mice on the basis of the methodologies described in the following sections.

Analyzed samples were deposited in the collection of the Animal Biodiversity Research Group of Universitat Autònoma de Barcelona. Voucher numbers of the specimens are listed in Appendix 1.

Histological analyses of mandible cross-sections

The characterization of the internal microstructure, the remodeling, and the growth rates of the mandible over ontogeny was approached through the analysis of histological cross-sections, in

accordance with Martinez-Maza et al. (2012) and Martínez-Vargas et al. (2017a). In order to analyze bone remodeling and growth rates, intraperitoneal injections of the fluorochrome Xylenol Orange (80 mg kg^{-1} of body weight, pH=7) were supplied *in vivo* to each animal. Shortly after their supply, vital dyes like Xylenol Orange fix to the mineralization front of the growing bone tissue, generating fluorescent labels visible under ultraviolet light (Pautke et al., 2005; van Gaalen et al., 2010). These labels appear as lines in histological cross-sections and correspond to the outline of the bone at the time of the fluorochrome injection. All mice received the first injection of Xylenol Orange at their 7^{th} day of postnatal life, and injections were then weekly supplied until one week before the stipulated date of euthanasia of each individual.

The 79 right dentary bones were dehydrated in graded ethanol, defatted in trichloroethylene and acetone, dried at 38–40°C in a stove, and embedded in a polyester resin. Histological cross-sections of 100µm (±10µm) thickness were obtained from four mandible regions using a diamond-tipped circular saw: diastema, first molar, second molar, and ascending ramus at the level of the condylar and angular processes (Fig. 1). Each thin section was ground, polished, and mounted on a slide. Histological cross-sections were photographed under natural and ultraviolet light with a digital camera coupled to an inverted fluorescent microscope (Zeiss Axiovert 35; Jena, Germany).

The pictures obtained under natural light were used to analyze the internal microstructure of the mandible of each animal, namely the spatial distribution of woven and parallel-fibered bone tissue in the different subregions of periosteal bone of each mandible region (Fig. 2). Woven bone tissue is characterized by collagen fibers with low ordered spatial arrangement, and by rounded osteocytic lacunae with random distribution (Fig. 3). Parallel-fibered bone tissue shows parallel arrangement of collagen fibers, and flattened osteocytic lacunae in ordered disposition (Fig. 3). The spatial distribution of both types of bone tissue observed in more than half of the mice of the same age and group was noted. In this way, the general histological patterns were established for each mandible subregion and PW, separately for Rb and St mice. Although this procedure might have excluded legitimate population variation, it was followed to provide the most representative and consistent histological pattern in each case.

The pictures obtained under ultraviolet light were used to analyze the bone remodeling and bone growth rates, based on the labeling patterns of Xylenol Orange. The presence, in the periosteum, of the fluorescent label corresponding to the last injection of fluorochrome, and bone in its periphery, was interpreted as evidence of bone deposition activity during the last week of life. The absence of this fluorescent label was associated with bone resorption, due to osteoclastic activity either in the periosteal or endosteal surfaces, or with dormant bone (i.e., cessation of bone growth) during that period. In order to determine the cause behind the absence of label in the periosteal surface, these results were combined with those from the analyses of bone surface histology (see the following section). Several subregions, based on the localization of observation points, were delimited in each mandible region to standardize and simplify the examinations (Figs. 4–7). A general pattern of fluorescent labeling was generated for each mandible subregion and PW, separately for St and Rb mice, which summarized the pattern found in more than half of the specimens in each case.

When periosteal bone deposition was evidenced, periosteal growth rates were calculated. The distance between the most peripheral fluorescent label and the periosteal bone surface was measured with the image processing package Fiji, a distribution of ImageJ (Schindelin et al., 2012). Several measurement points were established over the cross-section outlines (Figs. 4–7). Since linear measurements are affected by measurement error (Bailey and Byrnes, 1990), three replicates of all measurements were performed by the same person (JMV) in a subsample of ten individuals. A model II one-way ANOVA was then conducted to assess intra-observer measurement error, namely to test whether variation among individuals was higher than variation among replicates (Arnqvist and Martensson, 1998), and statistical significance was corrected with the sequential Bonferroni correction (Holm, 1979; Rice, 1989). Owing to the fact that variation among individuals significantly exceeded variation among replicates ($F = 4.5–5547.0$; $P<0.01$ in all measurements), intra-observer measurement error was considered negligible and measurements were taken once from all individuals by the same person (JMV). Daily rates of periosteal bone growth (in $\mu m\ day^{-1}$) corresponding to the last week of life were obtained dividing the distances by seven (i.e., the days elapsed between the date of the last injection of Xylenol Orange and the date of euthanasia). Adjacent measurement points showing similar growth rates over ontogeny were grouped, so that different subregions were delimited in each

mandible region (Figs. 4–7). For each individual mouse, the mean periosteal growth rate of each mandible subregion was calculated by averaging the growth rates corresponding to the measurement points included in the subregion in question. Then, the mean values of each subregion were further averaged among the individuals of both the same group and age, and the standard deviations were also obtained. The mean bone growth rates of all subregions were compared between Rb and St mice of the same age with the non-parametric Mann-Whitney U test, since Shapiro-Wilk W test revealed that the data deviated significantly from a normal distribution. Due to the large number of entries, the sequential Bonferroni correction was used to correct the statistical significances of the comparisons (Holm, 1979; Rice, 1989).

Histological analyses of mandible surfaces

The characterization of the ontogenetic remodeling patterns of the mandible was approached through the histological analysis of bone surfaces. Since the remodeling patterns of the left and right mandible sides of each individual were comparable, the left dentary bones from the 79 specimens were used for the analysis. The labial and lingual surfaces of the bones were coated with gold or platinum with sputter coaters (SC510 BioRad; Hercules, USA; Emitech K550X; Kent, UK), and examined with a reflected light microscope (Zeiss Axio Imager.A1; Goettingen, Germany) at 100x and 200x. The two types of remodeling fields were identified based on characteristic histological microfeatures (Bromage, 1989; Bloom and Fawcett, 1994; Martinez-Maza et al., 2010; Martínez-Vargas et al., 2017b). Bone deposition fields show packs of collagen fibers with parallel and ordered disposition, and predominant orientation (Fig. 8). Bone resorption fields display randomly distributed concavities, named Howship's lacunae, of variable size and irregular shapes (Fig. 8). Outlines of the labial and lingual views of each dentary bone were traced on paper, and the spatial distribution of the two types of remodeling fields observed in each specimen was mapped in these templates. As a result, the remodeling patterns of both mandible surfaces were obtained for each individual. Histological data was discarded whenever the identification of bone remodeling fields could not be performed with certainty. The remodeling patterns observed in more than half of the specimens of both the same group and age were represented in new outlines (see Martinez-Maza et al., 2013, 2015). In this way, the

general bone remodeling patterns of the mandible were established for each age class within each mouse group. Again, this procedure was followed to provide the most representative and consistent remodeling pattern in each case.

Geometric morphometric analyses of mandible form

The characterization of the ontogenetic variation of mandible form was approached through geometric morphometrics. Images of the lingual surfaces of the 158 right and left dentary bones, along with a scale bar, were obtained with an image scanner (Epson Perfection V350 Photo). Eighteen two-dimensional landmarks were digitized twice in each scaled image by the same person (JMV) using tpsDig2 (Rohlf, 2010) (Fig. 1). Geometric morphometric analyses were conducted with MorphoJ, ver. 1.06d (Klingenberg, 2011), and with the geomorph package in R, ver. 3.3.3 (R Core Team, 2016; Adams et al., 2017).

Size of each dentary bone was estimated as its centroid size. All landmark configurations were superimposed with a generalized Procrustes fit and projected onto the shape tangent space (Rohlf and Slice, 1990). The resulting landmark coordinates (i.e., Procrustes coordinates) only accounted for shape variation (Dryden and Mardia, 1998; Klingenberg and McIntyre, 1998). The sample was split into two datasets according to karyotype (St/Rb), which were further subdivided into seven datasets according to age (2^{nd}–8^{th} PW). Seven additional datasets were created by grouping St and Rb mice of the same age (Table 1).

Centroid size and Procrustes coordinates were respectively subjected to two-factor and Procrustes analyses of variance (ANOVAs) in all datasets (Klingenberg et al., 2002). Individual and side were the random and fixed main effects, respectively. The former represents variation among specimens (i.e., symmetric component of variation), the latter represents directional asymmetry, and their interaction stands for fluctuating asymmetry (i.e., asymmetric component of variation) (Mardia et al., 2000; Klingenberg et al., 2002). Mouse group and age were the additional main effects. The residual variation between replicates was the measurement error (Klingenberg and McIntyre, 1998). Subsequent analyses were conducted only with the symmetric component of variation.

Mean centroid size and the corresponding standard deviation were calculated among individuals of both the same group and age, for the dentary bone and separately for the two main regions commonly defined in the mouse mandible: the alveolar region (anterior region) and the ascending ramus (posterior region). Ontogenetic allometry was assessed through multivariate regressions of shape onto centroid size in each mouse group (Monteiro, 1999). Statistical significance of the regressions was obtained through permutation tests with 10,000 iterations (Good, 1994). Since allometry was found to be significant in both groups, subsequent analyses were based on both raw data (i.e., data not corrected for allometry) and size-corrected data (i.e., data corrected for allometry), unless there was no interest in removing the allometric effect or in analyzing raw data. Difference in the slope of the allometric regressions between Rb and St mice was assessed with an ANOVA for a homogeneity of slopes test, using the procD.lm function in geomorph. Differences in the length and orientation of the allometric trajectories between both mouse groups were tested with the advanced.procD.lm function in geomorph.

A between-group principal component analysis (PCA) was conducted by running a PCA on the covariance matrix of the group averages (14 groups, according to the combinations of mouse group and time point as grouping factors) and then using the resulting PC coefficients with the raw data of the whole sample, in order to examine the axes of greater shape variation and visualize potential separation among groups (Boulesteix, 2005; Mitteroecker and Bookstein, 2011; Franchini et al., 2016). A plot of relative warps in size-shape space was obtained by adding the logarithm of CS to the shape variables and then performing a PCA, with the aim of helping visualize allometric trajectories and potential non-random patterns within each group (Mitteroecker et al., 2004; Fruciano et al., 2012). Correlation coefficients (r) were calculated between the covariance matrices of St and Rb mice of the same age. Canonical variate analyses (CVAs) were conducted to further explore shape differences and calculate Procrustes distances between the two groups of mice in each postnatal week. Using raw data, CVAs were also conducted among age classes within each mouse group. Statistical significance of the correlation coefficients and Procrustes distances resulted from permutation tests with 10,000 permutation rounds (Good, 1994).

A multivariate matrix of variables was obtained by coding, for the specimens with known karyotype, each translocation as a three-state variable (0: absent, 1: heterozygous, 2: homozygous). This matrix was then used in a partial least squares (PLS) analysis, after correcting for the allometric effect, to identify patterns of covariation between mandible shape and Rb translocations.

The ontogenetic trajectories of the two mouse groups were compared in terms of length, shape and orientation using the trajectory.analysis function in geomorph (Collyer and Adams, 2013).

The hypothesis of organization of the mouse mandible into the alveolar region and ascending ramus modules was assessed. Although this modularity hypothesis is not universally supported and several others could be considered equally plausible (see Zelditch et al., 2008, 2009), it has been a favored hypothesis of mandible modularity (Zelditch et al., 2009) widely tested and validated among adult mice (Klingenberg et al., 2003; Fruciano et al., 2013). Thus, it was considered of interest to assess whether this hypothesis was also supported during the early postnatal ontogeny of the mouse. Since the RV coefficient (Escoufier, 1973) has been remarked to be adversely affected by sample size and the number of variables (Fruciano et al., 2013; Adams, 2016), the degree of integration of the mandible was assessed using the covariance ratio (CR) coefficient, which is not affected by these data attributes (Adams, 2016). Both for raw and size-corrected data from each group, two datasets were created by grouping different age classes (2^{nd}–4^{th} PW and 5^{th}–8^{th} PW), in order to test the modular organization. The chosen threshold aimed to address whether the magnitude of mandible integration around weaning (i.e., 2^{nd}–4^{th} PW) differed from that after weaning (i.e., 5^{th}–8^{th} PW), also coinciding with the attainment of sexual maturity in the house mouse (i.e., 5^{th}–6^{th} PW). In all four datasets, the CR coefficient was calculated between two subsets of eight and ten spatially contiguous landmarks, corresponding with the two mandible modules (Fig. 1). Statistical significance of the CR coefficients resulted from permutation tests with 1,000 permutation rounds (Adams, 2016).

Ethics statement

Animal collection permits were granted from the Departament d'Agricultura, Ramaderia, Pesca, Alimentació i Medi Natural (Direcció General de Medi Natural i Biodiversitat) of the Generalitat de Catalunya (Government of Catalonia; Catalonia, Spain). The protocols followed in this study were

ethically approved by the Comissió d'Ètica en l'Experimentació Animal i Humana (CEEAH) of the Universitat Autònoma de Barcelona (Barcelona, Spain). These protocols adhered to the legal requirements established by the Departament d'Agricultura, Ramaderia, Pesca, Alimentació i Medi Natural of the Generalitat de Catalunya (Permit Number: DAAM 6328), and to the AAA's Guiding Principles in the Care and Use of Animals. Animals were handled in strict compliance with the guidelines approved by these entities.

RESULTS

Internal microstructure of the mandible

The diastema of St and Rb mice always exhibited woven bone tissue in the dorsal and ventral portions. In the two mouse groups, both woven and parallel-fibered bone tissue were identified in the labial diastema subregion especially towards the end of the period, although the spatial distribution and timing differed, and in the lingual diastema subregion during most of the period (Tables 2 and 3).

The first and second molar regions showed woven bone tissue between the 2nd and 5th PW in both groups. While Rb mice generally also displayed this pattern over the following weeks, St mice usually displayed both bone tissue types together in the two molar regions from the 6th PW onwards (Tables 2 and 3).

The whole ascending ramus of St and Rb mice showed woven bone tissue alone until the 4th and 5th PW, respectively. Afterwards, both groups exhibited parallel-fibered bone surrounded by woven bone in the ventral ascending ramus, and differed in the histological pattern of the condylar process (Tables 2 and 3).

Remodeling and growth rates of the mandible from fluorescent bone labeling

Endosteal resorption was evident in the ventral subregion of the diastema of Rb and St mice between the 2nd and 4th PW, although the two groups differed in the particular spatial distribution of this remodeling activity (Tables 4 and 5). Endosteal resorption was also detected in the ventral half of

both molar regions in both mouse groups, just during the 2nd PW in St mice but up to the 3rd PW in Rb mice, although this activity was spatially more confined in Rb mice (Tables 4 and 5).

Absence of fluorescent labeling, likely due to dormant bone, was noticed in different subregions of the periosteal surface of the diastema in each mouse group from the 6th PW onwards (Tables 4 and 5). The first molar region of Rb and St mice lacked the fluorescent label along the dorsal half of the lingual area (points 15-17), initially due to dormant bone and afterwards to bone resorption (Tables 4 and 5). As for the second molar region, periosteal bone resorption was observed in the dorsal half of the labial portion (points 1-3) from the 4th PW in Rb mice, but over the entire study period in St mice. This activity was also detected in the dorsal half of the lingual portion (points 13-14) from the 5th and 6th PW onwards in St and Rb mice, respectively, and generally was more ubiquitous among St mice (Tables 4 and 5). Regarding the ascending ramus, the labial area of the condylar tip (points 1-3) did not show fluorescent label from the 3rd and 4th PW onwards in St and Rb mice respectively, but only Rb mice displayed evidence of periosteal resorption. This remodeling activity was also detected in the ventral area of the ascending ramus (points 4-16) in both groups towards the end of the period, although it was more noticeable in St mice (Tables 4 and 5).

In the four mandible regions and both mouse groups, rates of periosteal bone deposition were relatively high in the 2nd PW, increased in the 3rd PW, and decreased progressively afterwards (Figs. 4–7, Table 6). Periosteal bone deposition both in St and Rb mice was relatively faster in the ventro-labial area of the diastema and the first molar region (points 6-11 in both cases), in the ventral area of the second molar region (points 6-10), and in the ventral portion of the ascending ramus (points 4-16) (Figs. 4–7, Table 6). No significant differences in mean periosteal bone growth rates were detected between Rb and St mice, after applying the sequential Bonferroni correction (Table 6).

Mandible remodeling patterns from surface histology

Regarding the remodeling pattern of the labial mandible surface, bone deposition fields were prevalent in both mouse groups over the entire study period, although the presence of bone resorption fields increased over time. In each PW, St and Rb mice exhibited a resorption field spreading from the base of the coronoid process towards the posterior region of the molars alveoli, although its extension

increased over time and varied between groups. From the 6th to the 8th PW, the two mouse groups showed a resorption field covering the region between the bases of the coronoid and condylar processes. Bone resorption was also detected in the base of their angular process in the 6th and 7th PW, and in the alveolus of their first molar in the 7th and 8th PW (Fig. 9). Some differences were detected between St and Rb mice, like the fact that in the 7th PW the alveolar bone of the second molar displayed resorption activity among Rb mice but not among St mice. In the 8th PW, bone resorption was detected in the base of the angular process of Rb mice but, instead, above the most concave point of the ventral mandible border in St mice (Fig. 9).

As for the remodeling pattern of the lingual surface of the mandible, bone deposition was the predominant activity throughout the study period in both groups, and was the only remodeling activity detected in the 2nd PW (Fig. 9). The ramal fossa of Rb and St mice displayed bone resorption activity in its anteroventral area in the 3rd PW, but in all its extension between the 6th and 8th PW. In the 4th PW, and from the 6th to the 8th PW, both groups showed a resorption field between the base of the coronoid process and the molar region. From the 6th to the 8th PW, St and Rb mice displayed one or more resorption fields extending over the molars alveoli, and in the 8th PW they also exhibited bone resorption in the base of the condylar process (Fig. 9). However, only St mice showed resorption activity below the coronoid process in the 3rd PW, and over the molars alveoli in the 5th PW. Instead, only Rb mice displayed a field of bone resorption below the coronoid process in the 5th PW and another one in the base of the condylar process in the 6th and 7th PW. In the 4th and 5th PW, resorption was just detected in the anteroventral area of the ramal fossa in Rb mice but, instead, in the entire ramal fossa in St mice (Fig. 9).

Histological data could not be obtained from the tips of the coronoid, condylar, and angular processes, and from the anteroventral region of the diastema.

Patterns of variation in mandible form

The two-factor and Procrustes ANOVAs conducted on the whole sample revealed significant variation among individuals, directional asymmetry, and fluctuating asymmetry in mandible size and shape, as well as negligible measurement error (Tables 7 and 8).

Significant differences in mandible size were detected among age classes within each mouse group (P<0.05). Instead, differences in mandible size between Rb and St mice of the same age were generally not significant (Fig. 10, Table 9). Ontogenetic size increase was relatively greater for the ascending ramus than for the alveolar region in both mouse groups (Table 9).

Mandible shape differences among age classes within each mouse group were statistically significant (P<0.05). The two mouse groups differed significantly in mandible shape from the 6th to the 8th PW (P<0.001).

According to the allometric regressions, both Rb and St mice exhibited a significant allometric component (P<0.001), and similar proportions of variance in shape accounted for by size variation (Rb: 39.46%; St: 35.77%). Both groups exhibited similar allometric shape changes over ontogeny, consisting of a relative shortening of the alveolar region and a relative increase in height and length of the ascending ramus (Fig. 11). A significant interaction between group and centroid size was revealed by the homogeneity of slopes test (F=3.019; P=0.008). The allometric trajectories of St and Rb mice differed significantly from parallel (θ=29.927; P=0.002), but did not differ in length (Δd=0.034; P=0.21).

The between-group PCA showed a gradation of consecutive age classes along the axis of the first between-group principal component (PC1), which accounted for 45.08% of total shape variation (Fig. 12). The axis of the second between-group principal component (PC2), explaining 13.80% of total shape variation, suggested late divergence (i.e., during the last age stages) between the two groups of mice (Fig. 12). The main shape changes associated with PC1 principally involved the posterior region of the mandible and the incisor alveolus, while shape changes linked to PC2 mainly involved the ascending ramus (Fig. 12). The PCA in size-shape space also revealed a gradation of consecutive age classes over the PC1 axis (84.56% of variation), and suggested a more discernible divergence between the two mouse groups towards the end of the period along the PC2 axis (3.05% of variation) (Fig. 13). The covariance matrices of Rb and St mice of the same age were positively and significantly correlated, but the low correlation coefficients highlighted the dissimilar patterns of morphological covariation between the two groups (Table 10). Procrustes distances between St and Rb mice were statistically significant in the 6th and 7th PW (Table 11). Statistically significant Procrustes distances

(P<0.05) also resulted from the comparison between consecutive age classes within each mouse group.

The PLS analysis revealed the existence of significant covariation between mandible shape and Rb translocations (RV=0.171; P<0.001). The first partial least squares (PLS1) accounted for 92.074% of covariation, and appeared to be more associated with the Rb translocations Rb(4.14) (PLS1 coefficient=0.487), Rb(12.13) (PLS1 coefficient=0.480), and Rb(5.15) (PLS1 coefficient=0.432). Similar mandible shape variation was associated with these three chromosomal reorganizations, and involved the posterior mandible region to a greater extent.

The ontogenetic trajectories of St and Rb mice did not differ in length (Δd=0.013; P=0.503) nor shape (D_P=0.203; P=0.944), but they did differ in their orientation (θ=34.017º; P=0.001). The ontogenetic trajectories were projected onto principal components of between-group shape variation to facilitate their interpretation (Fig. 14).

According to the CR coefficients, the magnitude of integration of the mandible was generally higher in the period between the 2nd and 4th PW than in the period from the 5th to the 8th PW, in both mouse groups (Table 12). The CR coefficients confirmed the modular organization of the mandible into the alveolar region and ascending ramus modules only in the case of St mice and particularly for the period ranging between the 5th and 8th PW (Table 12).

Timing of tooth eruption

In the 2nd PW, just the cusps of the first molar (m1) and second molar (m2) could be seen in lingual mandible view in 33.33% of St mice and 28.57% of Rb mice. The cusps of m1 and m2, but also the basal portion of the m1 crown, were erupted in 33.33% of St mice but in 57.14% of Rb mice. Eruption of the crowns of m1 and m2 seemed to be complete in the remaining 33.33% of St mice and 14.29% of Rb mice. In the 3rd PW, the basal portion of the m2 crown was emerged through the alveolar bone in all St and Rb mice. Also, the cusps of the third molar (m3) were visible in lingual view in 57.14% of Rb and St mice, and in dorsal view in the remaining 42.86% of both groups. In the 4th PW, eruption of all molars appeared to be complete in both mouse groups. The eruption of the incisors looked

complete in St and Rb mice by the 3rd PW, and no evident differences in their pattern of eruption were noticed between the two groups.

DISCUSSION

Mandible growth from a histological perspective

According to Amprino's rule (1947), woven bone is typical of the early life stages characterized by fast bone deposition and growth, and ontogenetically precedes parallel-fibered bone, which results from slower bone deposition. Our analyses of the internal microstructure of the mandibles revealed that, both in St and Rb mice, woven bone tissue was prevalent in the first half of the study period, while the presence of parallel-fibered bone tissue was more evident in the second half. Also, periosteal bone deposition appeared to be relatively faster at the beginning of the study period and started decelerating notably after the 4th PW. The histological and growth rate data also revealed that, in both groups, the range of growth rates corresponding to the sole deposition of woven bone had a higher upper threshold than the range associated with the deposition of woven and parallel-fibered bone together. Nonetheless, the lower threshold of these ranges was quite similar, so an important overlap was detected between the ranges of growth rates corresponding to each histological characterization. Therefore, our results support that Amprino's rule (1947) applies to the growth of the mouse mandible, but also show that this rule should be carefully considered since bone histology may not always be an unequivocal predictor of the speed of bone growth (see also Castanet et al., 2000; Starck and Chinsamy, 2002; de Margerie et al., 2004).

The ontogenetic transition from woven to parallel-fibered bone tissue, which is considered to result from the deceleration of bone deposition, has been regarded as an indicator of bone maturation (Amprino, 1947; de Ricqlès, 1975; Currey, 2002). Based on this assumption, our results revealed that the transformation from 'immature' to 'mature' bone tissue occurred in an anteroposterior direction in both groups of mice: their diastema region started maturing early, while their molar and especially their ascending ramus regions started maturing some weeks later. While this anteroposterior histological transformation was also described in the mandible of laboratory mice of the C57BL/6J

inbred strain, in that case the pattern of maturation of the entire molar region resembled more the pattern of the diastema than that of the ascending ramus, which was interpreted as supporting the existence of two main mandible modules (i.e., alveolar region and ascending ramus) at the histological level (Martinez-Maza et al., 2012). Instead, our histological results suggest a more anterior boundary between potential histological modules, apparently located between the diastema and the molar region. Our results also suggest that histological maturation of the mandible might be slightly faster among St mice, since they showed a higher prevalence of parallel-fibered bone tissue, particularly in the molar region, and an earlier presence of that bone tissue type in certain areas of the diastema and the ascending ramus.

Early ventral cortical drift is expected both in the diastema and molar regions of St and Rb mice, according to their patterns of fluorescent labeling, since the ventral area of these mandible regions displayed endosteal bone resorption and relatively fast periosteal bone deposition at the beginning of the ontogenetic period analyzed. Nonetheless, the two groups might differ in the exact spatial direction of this cortical drift as well as in the cortical thickness in these mandible regions, since differences were detected in the specific patterns of presence and absence of the fluorescent label. Synchronized development of the mandible and teeth is essential to preserve the functionality of these elements (Fraser et al., 2009). In the mouse, the pattern of dental development is indeed related to mandible shape ontogeny over postnatal life (Swiderski and Zelditch, 2013), which leads to anticipate that the timing of tooth eruption should be also linked to mandible remodeling. The effective adult mouse dentition (i.e., incisors, m1, and m2) is in place around the 21st postnatal day, while the eruption of m3 is complete five days later (Chlastaková et al., 2011; Swiderski and Zelditch, 2013). The finding that ventral drift of m1 and m2 alveoli occurred up to the end of the 3rd PW in Rb mice, but just until the end of the 2nd PW in St mice, initially suggested faster development and eruption of these molars among St mice. The fact that the eruption of m1 and m2 in the 2nd PW appeared to be slightly faster in St mice supports the link between dental development and mandible remodeling. However, growth rates of both molar regions were not significantly different between the two groups of mice. The detection of ventral cortical drift in the diastema of St and Rb mice between the 2nd and 4th PW

indicates equivalent temporal patterns of remodeling, and suggests that the roots of the mouse incisors probably achieve their target thickness right after weaning.

Considering that deposition and resorption fields on bone surface respectively face and oppose the direction of bone growth (Enlow and Hans, 1996), the similarities between St and Rb mice in the patterns of bone surface histology and fluorescent bone labeling allow us to infer a shared pattern of ontogenetic mandible growth. In addition to the ventral cortical drift taking place in the anterior mandible region during the initial weeks, their diastema underwent an increase in bilateral width during the whole period, while their whole molar region also expanded bilaterally over the first weeks but it grew laterally on its anterior part and narrowed on its posterior part during the last weeks. Also, their ascending ramus displayed lateral growth in the area between the condylar and angular processes during most of the period, and in the anterior margin of the coronoid process during the last weeks. The data based on fluorescent labeling indicated medial growth of the portion between the tips of the coronoid and condylar processes at the end of the study period, and narrowing of the area below the coronoid process and posterior to the molars row most of the time. However, the numerous dissimilarities between Rb and St mice in the patterns of bone remodeling, according to both techniques, are supposed to reflect differences in their temporospatial patterns of mandible growth, which might account for phenotypic variation.

The combination of the results from the histological analyses of bone cross-sections and bone surfaces revealed that the presence of bone resorption fields on mandible surface was not always linked to the absence of fluorescent label in the histological cross-sections. Conversely, the lack of fluorescent labeling not always coincided with the detection of resorption fields. At this point, it should be recalled that the remodeling patterns from bone surface histology corresponded to the moment when the animals died, while the analyses of bone remodeling and growth rates from histological cross-sections were based on a fluorochrome supplied and attached to the bone one week before the date of euthanasia of the animals. Therefore, the first incongruence might be due to the fact that the resorption activity that was supposed to be carried out by osteoclasts during the last week of life probably was not intense enough to remove the labeled bone. The second incongruence might result from the presence of dormant bone at least at the time of the fluorochrome injection. In view of

our results, the present study evidences that the combination of different histological methodologies to approach bone growth is likely to more effectively help understand this biological process.

Mandible growth from a morphometric perspective

Despite the allometric trajectories of Rb and St mice were not parallel, the angle between them was relatively small, which concurs with the fact that their mandibles displayed similar shape changes dependent on size. The stimulation of bone deposition vs. bone resorption depends to a great extent on whether the mechanical strains exerted by muscles on bones surpass or not a certain threshold, respectively (Robling et al., 2006; Herring, 2011; Burr and Allen, 2013). In this way, the bone remodeling mechanism allows the skeleton to adapt to the changes in muscular loading (Burr and Allen, 2013). The post-weaning change of diet promotes an alteration in the fiber properties and forces of the masticatory muscles, causing an increase in the mechanical loading exerted by these muscles on the mandible that contributes to the correct performance of the gnawing and chewing functions (Suzuki et al., 2007; Enomoto et al., 2010). Bearing this in mind, the relatively greater growth of the ascending ramus over ontogeny in both mouse groups could be due to the greater influence of post-weaning muscular loading on the remodeling of this mandible region, since it is the attachment site for most of the masticatory muscles. Although the greater abundance of bone resorption fields in the ascending ramus over ontogeny could seem contradictory, it might be the outcome of the diverse functions, and interactions with the bone, of the different masticatory muscles (see Herring, 2011). Nonetheless, muscular loading would trigger more intense deposition activity, at least in dorsoventral and/or anteroposterior direction, in the ascending ramus than in the alveolar region.

Ontogenetic shape changes of the ascending ramus were of greater magnitude than those of the alveolar region in both mouse groups, in accordance with prior studies (see Burgio et al., 2012; Martínez-Vargas et al., 2014). Bone remodeling is expected to affect all bone dimensions, including both bone outline and bone surface, on which the morphometric and certain histological analyses were respectively based in the present study. Therefore, the fact that the spatial distribution of bone remodeling fields exhibited greater inter-individual variation in the posterior mandible region, in each age class within each mouse group, might account for the higher magnitude of shape variation in the

ascending ramus over ontogeny. At the same time, this greater inter-individual variation in the remodeling patterns of the ascending ramus might be linked to the high variety of muscular forces that could be exerted on this region. Since bone responsiveness to mechanical loading has a genetic basis, inter-individual variation in the sensitivity of the mandible to changes in muscular loading might also underlie that finding (see Judex et al., 2002). Furthermore, genetic variation of mouse mandible shape is driven by many quantitative trait loci (QTLs) clustered into two morphogenetic components corresponding to the alveolar region and ascending ramus, and the latter is controlled by more QTLs (see Ehrich et al., 2003; Cheverud et al., 2004; Klingenberg et al., 2004; Burgio et al., 2012). Therefore, the genetic independence and different polygenic architecture of the anterior and posterior mandible regions might also account for the independence of the morphological changes occurring in each region.

According to the comparison of the ontogenetic trajectories, Rb and St mice did not differ in the amount of mandible shape changes at the ontogenetic level, but they did differ in the direction of morphological change. The observation that St and Rb mice particularly differed in the main patterns of shape variation of the ascending ramus over ontogeny suggests a role of Rb translocations, and concurs with previous studies also including Rb mice. Muñoz-Muñoz et al. (2011) found that shape divergence of the alveolar region between adult Rb and St mice from the 'Barcelona' Rb system and surrounding St populations was correlated only with their geographical distances, while shape divergence between their ascending ramus was correlated both with karyotype differences and geographical distances. Similarly, Franchini et al. (2016) analyzed two metacentric races of mice and detected a significant association between morphometric and geographic distances regarding the alveolar region, whereas in the case of the ascending ramus significant associations were found between morphometric and both genetic and karyotypic distances. Therefore, the alveolar region of the mouse mandible is considered to be relatively more influenced by environmental factors than the ascending ramus (Franchini et al., 2016). At this point, it should be recalled that the Rb and St mice used in the present study were reared under equivalent conditions. Also, it should be taken into account that Rb translocations reduce meiotic recombination as well as affect gene architecture and expression, and that more QTLs are involved in the shape changes of the ascending ramus than of the

alveolar region (Ehrich et al., 2003; Navarro and Barton, 2003; Klingenberg et al., 2004; Capilla et al., 2014; Franchini et al., 2016). Bearing all this in mind, it could be suggested that the presence of Rb translocations, but especially Rb(4.14), Rb(12.13), and Rb(5.15) in particular, might explain the greater shape divergence of the ascending ramus between our St and Rb mice. In addition, the fact that mandible shape differences between Rb and St mice were statistically significant from the 6th PW (i.e., when the house mouse attains sexual maturity), which is also evident from the ontogenetic trajectories, suggests that this milestone would be the starting point of the significant mandible shape differences often detected between adult St and Rb mice (see Martínez-Vargas et al., 2014).

The ontogenetic decrease in the CR coefficient detected in both mouse groups indicates relatively lower strength of integration between the alveolar region and the ascending ramus modules over ontogeny. This observation agrees with previous studies showing an ontogenetic increase in the level of modularity (for review, see Goswami et al., 2014). The hypothesis of modularity tested was previously confirmed both in mice with and without Rb translocations from the same zone of Rb polymorphism (Martínez-Vargas et al., 2014), although differences in the level of modularity according to such hypothesis have been also documented between St and Rb mice (Fruciano et al., 2013; Martínez-Vargas et al., 2014). However, the modular organization into the alveolar region and ascending ramus was only validated in St mice in the present study. This result suggests that the presence of Rb translocations might modify the ontogenetic patterns of morphological covariation of the mandible typical of the subspecies. The reduction in the recombination rate prompted by Rb translocations might cause a decrease in gene exchange (Franchini et al., 2010), and could prompt the fixation of certain alleles with specific pleiotropic effects (Franchini et al., 2016). This decrease in meiotic recombination may also entail the linkage of genes underlying shape variation of the two mandible modules (Franchini et al., 2016). Furthermore, the redistribution of chiasmata caused by Rb translocations may disrupt linkage groups including several alleles of loci with an effect on only one of the mandible modules. Eventually, these scenarios would entail a relative decrease in the strength of intra-modular integration and, thus, in the level of modularity during the early postnatal ontogeny of Rb mice. The hypothesis of modularity was validated in St mice after weaning, which suggests that

the functional constraints induced on the mandible by the post-weaning change of diet might underlie the relatively higher within-modules integration after weaning.

Robertsonian translocations and mandible growth

The comprehensive evaluation of our histological and morphometric results seems to validate the hypothesis that the early postnatal growth of the mandible differs to some extent between our St and Rb mice. However, the differences in mandible form between these mouse groups are not likely to be attributable solely to their dissimilarities in the spatial distribution of the two types of bone remodeling fields on mandible surface over ontogeny (see Brachetta Aporta et al., 2014, for a similar case).

Phenotypic variation in animals from natural populations is known to result from a mix of genetic and environmental factors (Renaud et al., 2010). Despite the mice used in the present study were born from wild females trapped in different localities, their early postnatal growth took place under the same conditions. Therefore, environmental factors with an influence on mandible growth, such as diet and the loading exerted by masticatory muscles depending on food consistency, are not likely to account for the differences in the patterns of mandible growth here detected between Rb and St mice. Instead, these dissimilarities are more likely to have a genetic basis.

Genetically-based phenotypic variation of the mouse mandible results from many genes with partly redundant and pleiotropic effects (Cheverud et al., 2004; Klingenberg et al., 2004). Compared to the original acrocentric chromosomes, metacentrics resulting from Rb translocations show substantial reduction in the number of meiotic crossovers, especially in the pericentromeric region, due to the redistribution of these recombinational events towards the telomeric regions (Castiglia and Capanna, 2002; Dumas and Britton-Davidian, 2002; Franchini et al., 2010; Capilla et al., 2014). As a result, Rb translocations could alter the genetic linkage, flow, and function of genes located in the chromosomes undergoing these rearrangements (Navarro and Barton, 2003). Although Rb translocations are considered to underlie skeletal form variation in adult mice (see Corti and Rohlf, 2001; Sans-Fuentes et al., 2009; Muñoz-Muñoz et al., 2011; Martínez-Vargas et al., 2014), few relations have been described between these spontaneous chromosomal reorganizations and bone growth before adulthood. Yet, mouse fetuses double heterozygous for the Rb translocations Rb(6.16) and Rb(16.17)

were found to display retarded and poorly ordered bone tissue development, diminished growth, decreased size, flattened snouts, and hypoplastic and smaller teeth (di Stefano and Provenza, 1993, 1994). This finding serves as a precedent to suggest that the differences here detected between the patterns of mandible growth of St and Rb mice might be due to alterations exerted by Rb translocations, and perhaps particularly by certain ones (i.e., Rb(4.14), Rb(12.13), and Rb(5.15)), on genes involved in the remodeling process of the mandible. Nevertheless, different allelic constitutions in each mouse group due to genetic drift or natural selection might also account to some extent for these differences.

The bone growth remodeling mechanism depends on the genetic program of osteoblasts and osteoclasts (Turner, 1998). However, the activities of these bone cells are also influenced by many genetically encoded signaling molecules such as hormones (Robling et al., 2006). Hormonal factors have been observed to mediate morphological changes in the craniofacial complex of the mouse and other mammals after birth (Fujita et al., 2004; Ramirez-Yañez et al., 2005). The growth hormone (GH) is essential for normal bone development and skeletal growth, and the dysfunction of the GH receptors, which are located in osteoblasts, causes decreased bone mineral content and disproportional skeletal growth (Sjögren et al., 2000; Ramirez-Yañez et al., 2005). The gene codifying for the GH receptor in the mouse is mapped very close to the centromere of chromosome 15 (Chr15: 3,317,760-3,583,492 bp, - strand) (Barton et al., 1989; Sjögren et al., 2000). Interestingly, this chromosome is involved in one of the Rb translocations described in the 'Barcelona' Rb system, Rb(5.15), which is found in a heterozygous or homozygous state in virtually all Rb mice included in the present study. Although no evident growth failure was detected among Rb mice, some results actually pointed to more retarded patterns of mandible growth and dental development in this mouse group. These observations support the chance that the Rb translocations of our Rb mice might alter the expression or function of certain molecules with an effect on the activity of bone cells, which would modify the temporospatial patterning and regulation of the mandible remodeling process over early postnatal ontogeny.

Sensitivity of murine bone to mechanical loading is considered to have a strong genetic component, which suggests that subtle changes in the ability of bones to respond to mechanical loading, and thus

in bone deposition rates during growth, could lead to significant differences in adult bone size and shape (Judex et al., 2002; Robling et al., 2003). Although the complete set of genes involved in skeletal mechanosensitivity has not been described yet, Robling et al. (2003) supported the existence of a genetic locus in mouse chromosome 4 that modulates bone sensitivity to mechanical strains. Again, chromosome 4 is involved in one of the Rb translocations present in the Rb system under study, Rb(4.14), also found in practically all Rb mice analyzed. Even though Rb and St mice had a common diet pattern, and thus the same ontogenetic pattern of muscular loading was expected to influence their mandibles, the dissimilarities in mandible growth detected between these mouse groups also suggest the existence of potential differences between them in bone mechanosensitivity.

The present study encourages further investigation into the genetic mechanisms directing and regulating the remodeling process and, thus, growth of bones over postnatal life. Particularly, further research would be required to elucidate which genes involved in the postnatal growth of the mouse mandible, among other bones, might be affected by particular Rb translocations occurring spontaneously. Work toward these goals could help to ascertain whether different karyotypic and/or genetic constitutions between St and Rb mice may truly underlie potential differences in bone growth and morphology between them, and therefore might account for their evolutionary phenotypic differentiation.

ACKNOWLEDGMENTS

We thank Dr. Nuria Medarde for her valuable contribution to the fieldwork and the karyotyping of the specimens, Ana Filipa Lopes Durão (Universitat Autònoma de Barcelona) for her assistance with the statistical analyses, Hayat Lamrous (Université Pierre et Marie Curie) for the obtainment of the histological cross-sections, and Dr. Joan M. Roure and Dr. Jordina Belmonte (Universitat Autònoma de Barcelona) for providing us with access to the reflected light microscope used for the analyses of bone surface histology. This study was conducted in the framework of the PhD program in Biodiversity from Universitat Autònoma de Barcelona. JMV receives a PIF grant from Universitat Autònoma de Barcelona.

LITERATURE CITED

Adams DC. 2016. Evaluating modularity in morphometric data: challenges with the RV coefficient and a new test measure. Methods Ecol Evol 7:565–572.

Adams DC, Collyer ML, Kaliontzopoulou A, Sherratt E. 2017. Geomorph: Software for geometric morphometric analyses. R package version 3.0.5. https://cran.r-project.org/package=geomorph.

Adolph S, Klein J. 1981. Robertsonian variation in *Mus musculus* from Central Europe, Spain, and Scotland. J Hered 72:219–221.

Amprino R. 1947. La structure du tissu osseux envisagee comme expression de differences dans la vitesse de l'accroissement. Arch Biol 58:315–330.

Arnqvist G, Martensson T. 1998. Measurement error in geometric morphometrics: empirical strategies to assess and reduce its impact on measures of shape. Acta Zool Academ Sci Hung 44:73–96.

Atchley WR, Hall BK. 1991. A model for development and evolution of complex morphological structures. Biol Rev Camb Philos Soc 66:101–157.

Bailey RC, Byrnes J. 1990. A new, old method for assessing measurement error in both univariate and multivariate morphometrics studies. Syst Zool 39:124–130.

Barton DE, Foellmer BE, Wood WI, Francke U. 1989. Chromosome mapping of the growth hormone receptor gene in man and mouse. Cytogenet Cell Genet 50:137–141.

Bloom W, Fawcett DW. 1994. A Textbook of Histology. 12th ed. New York: Chapman & Hall.

Boulesteix A-L. 2005. A note on between-group PCA. Int J Pure Appl Math 19:359–366.

Brachetta Aporta N, Martinez-Maza C, Gonzalez PN, Bernal V. 2014. Bone modeling patterns and morphometric craniofacial variation in individuals from two prehistoric human populations from Argentina. Anat Rec 297:1829–1838.

Bromage TG. 1989. Ontogeny of the early hominid face. J Hum Evol 18:751–773.

Burgio G, Baylac M, Heyer E, Montagutelli X. 2012. Exploration of the genetic organization of morphological modularity on the mouse mandible using a set of interspecific recombinant congenic strains between C57BL/6 and mice of the *Mus spretus* species. G3 2:1257–1268.

Burr DB, Allen MR. 2013. Basic and Applied Bone Biology. Academic Press.

Capanna E, Civitelli MV, Castaldi M. 1974. Una popolazione appenninica di *Mus musculus* L. caratterizzata da un cariotipo a 22 cromosomi. Rend Lincei Sci Fis Nat 54:981–984.

Capilla L, Medarde N, Alemany-Schmidt A, Oliver-Bonet M, Ventura J, Ruiz-Herrera A. 2014. Genetic recombination variation in wild Robertsonian mice: on the role of chromosomal fusions and Prdm9 allelic background. Proc Biol Sci 281:20140297. DOI: 10.1098/rspb.2014.0297.

Castanet J, Rogers KC, Cubo J, Boisard JJ. 2000. Periosteal bone growth rates in extant ratites (ostriche and emu). Implications for assessing growth in dinosaurs. C R Acad Sci III, Sci Vie 323:543–550.

Castiglia R, Capanna E. 2002. Chiasma repatterning across a chromosomal hybrid zone between chromosomal races of *Mus musculus domesticus*. Genetica 114:35–40.

Cheverud JM, Ehrich TH, Vaughn TT, Koreishi SF, Linsey RB, Pletscher LS. 2004. Pleiotropic effects on mandibular morphology II: differential epistasis and genetic variation in morphological integration. J Exp Zool B Mol Dev Evol 302:424–435.

Cheverud JM, Routman EJ, Irschick DJ. 1997. Pleiotropic effects of individual gene loci on mandibular morphology. Evolution 51:2006–2016.

Chlastaková I, Lungová V, Wells K, Tucker AS, Radlanski RJ, Míšek I, Matalová E. 2011. Morphogenesis and bone integration of the mouse mandibular third molar. Eur J Oral Sci 119:265–274.

Chmátal L, Gabriel SI, Mitsainas GP, Martínez-Vargas J, Ventura J, Searle JB, Schultz RM, Lampson MA. 2014. Centromere strength provides the cell biological basis for meiotic drive and karyotype evolution in mice. Curr Biol 24:2295–2300.

Collyer ML, Adams DC. 2013. Phenotypic trajectory analysis: comparison of shape change patterns in evolution and ecology. Hystrix 24:75–83.

Committee on Standardized Genetic Nomenclature for Mice. 1972. Standard karyotype of the mouse, *Mus musculus*. Heredity 63:69–72.

Corti M, Rohlf FJ. 2001. Chromosomal speciation and phenotypic evolution in the house mouse. Biol J Linn Soc Lond 73:99–112.

Currey JD. 2002. Bones. Structure and Mechanics. New Jersey: Princeton University Press.

de Buffrénil V, Pascal M. 1984. Croissance et morphogénèse postnatales de la mandibule du vison (*Mustela vison* Schreiber): données sur la dynamique et l'interprétation fonctionnelle des dépôts osseux mandibulaires. Can J Zool 62:2026–2037.

de Margerie E, Robin JP, Verrier D, Cubo J, Groscolas R, Castanet J. 2004. Assessing a relationship between bone microstructure and growth rate: a fluorescent labelling study in the king penguin chick (*Aptenodytes patagonicus*). J Exp Biol 207:869–879.

de Ricqlès A. 1975. Recherches paléohistologiques sur les os longs des tétrapodes. VII- Sur la classification, la signification fonctionnelle et l'histoire des tissus osseux de tétrapodes (première partie: structures). Annls Paléont (Vert) 61:51–129.

di Stefano TV, Provenza DV. 1993. Molar odontogenesis in the trisomic 16 mouse. Arch Oral Biol 38:793–802.

di Stefano TV, Provenza DV. 1994. Osteogenesis of the mandibular arch in Ts16 mice. Arch Oral Biol 39:121–133.

Dryden IL, Mardia KV. 1998. Statistical Shape Analysis. Chichester: John Wiley & Sons.

Dumas D, Britton-Davidian J. 2002. Chromosomal rearrangements and evolution of recombination: comparison of chiasma distribution patterns in standard and Robertsonian populations of the house mouse. Genetics 162:1355–1366.

Ehrich TH, Vaughn TT, Koreishi SF, Linsey RB, Pletscher LS, Cheverud JM. 2003. Pleiotropic effects on mandibular morphology I. Developmental morphological integration and differential dominance. J Exp Zool B Mol Dev Evol 296:58–79.

Enlow DH. 1963. Principles of Bone Remodeling: An Account of Post-Natal Growth and Remodeling Process in Long Bone and the Mandible. Springfield: Charles C. Thomas

Enlow DH. 1982. Handbook of Facial Growth. Philadelphia: WB Saunders.

Enlow DH, Hans MG. 1996. Essentials of Facial Growth. Philadelphia: WB Saunders.

Enomoto A, Watahiki J, Yamaguchi T, Irie T, Tachikawa T, Maki K. 2010. Effects of mastication on mandibular growth evaluated by microcomputed tomography. Eur J Orthod 32:66–70.

Escoufier Y. 1973. Le traitement des variables vectorielles. Biometrics 29:751–760.

Ford CE. 1966. The use of chromosome markers. In: Micklem HS, Loutit JF, editors. Tissue Grafting and Radiation. New York: Academic Press. p 197–206.

Franchini P, Colangelo P, Meyer A, Fruciano C. 2016. Chromosomal rearrangements, phenotypic variation and modularity: a case study from a contact zone between house mouse Robertsonian races in Central Italy. Ecol Evol 6:1353–1362.

Franchini P, Colangelo P, Solano E, Capanna E, Verheyen E, Castiglia R. 2010. Reduced gene flow at pericentromeric loci in a hybrid zone involving chromosomal races of the house mouse *Mus musculus domesticus*. Evolution 64:2020–2032.

Fraser GJ, Hulsey CD, Bloomquist RF, Uyesugi K, Manley NR, Streelman JT. 2009. An ancient gene network is co-opted for teeth on old and new jaws. PLoS Biol 7:e31.

Fruciano C, Franchini P, Meyer A. 2013. Resampling-based approaches to study variation in morphological modularity. PLoS ONE 8:e69376.

Fruciano C, Tigano C, Ferrito V. 2012. Body shape variation and colour change during growth in a protogynous fish. Environ Biol Fish 94:615–622.

Fujita T, Ohtani J, Shigekawa M, Kawata T, Kaku M, Kohno S, Tsutsui K, Tenjo K, Motokawa M, Tohma Y, Tanne K. 2004. Effects of sex hormone disturbances on craniofacial growth in newborn mice. J Dent Res 83:250–254.

Garagna S, Page J, Fernandez-Donoso R, Zuccotti M, Searle JB. 2014. The Robertsonian phenomenon in the house mouse: mutation, meiosis and speciation. Chromosoma 123:529–544.

Good P. 1994. Permutation Tests: A Practical Guide to Resampling Methods for Testing Hypotheses. New York: Springer.

Goswami A, Smaers JB, Soligo C, Polly PD. 2014. The macroevolutionary consequences of phenotypic integration: from development to deep time. Philos Trans R Soc Lond B Biol Sci 369:20130254.

Gropp A, Winking H. 1981. Robertsonian translocations: cytology, meiosis, segregation patterns and biological consequences of heterozygosity. Symp Zool Soc Lond 47:141–181.

Gündüz İ, López-Fuster MJ, Ventura J, Searle JB. 2001. Clinal analysis of a chromosomal hybrid zone in the house mouse. Genet Res 77:41–51.

Gündüz İ, Pollock CL, Giménez MD, Förster DW, White TA, Sans-Fuentes MA, Hauffe HC, Ventura J, López-Fuster MJ, Searle JB. 2010. Staggered chromosomal hybrid zones in the house mouse: relevance to reticulate evolution and speciation. Genes 1:193–209.

Hauffe HC, Giménez MD, Searle JB. 2012. Chromosomal hybrid zones in the house mouse. In: Macholán M, Baird SJE, Munclinger P, Piálek J, editors. Evolution of the House Mouse. Cambridge: Cambridge University Press. p 407–430.

Hausser J, Fedyk S, Fredga K, Searle JB, Volobouev V, Wojcik JM, Zima J. 1994. Definition and nomenclature of the chromosome races of *Sorex araneus*. Folia Zool 43:1–9.

Hayes LD. 2000. To nest communally or not to nest communally: a review of rodent communal nesting and nursing. Anim Behav 59:677–688.

Herring SW. 2011. Muscle-bone interactions and the development of skeletal phenotype: jaw muscles and the skull. In: Hallgrimsson B, Hall BK, editors. Epigenetics: Linking Genotype and Phenotype in Development and Evolution. Berkeley: University of California Press. p 221–237.

Holm S. 1979. A simple sequentially rejective multiple test procedure. Scand J Statist 6:65–70.

Judex S, Donahue LR, Rubin C. 2002. Genetic predisposition to low bone mass is paralleled by an enhanced sensitivity to signals anabolic to the skeleton. FASEB J 16:1280–1282.

Klingenberg CP. 2011. MorphoJ: an integrated software package for geometric morphometrics. Mol Ecol Resour 11:353–357.

Klingenberg CP, Barluenga M, Meyer A. 2002. Shape analysis of symmetric structures: quantifying variation among individuals and asymmetry. Evolution 56:1909–1920.

Klingenberg CP, Leamy LJ, Cheverud JM. 2004. Integration and modularity of quantitative trait locus effects on geometric shape in the mouse mandible. Genetics 166:1909–1921.

Klingenberg CP, McIntyre GS. 1998. Geometric morphometrics of developmental instability: analyzing patterns of fluctuating asymmetry with Procrustes methods. Evolution 52:1363–1375.

Klingenberg CP, Mebus K, Auffray J-C. 2003. Developmental integration in a complex morphological structure: How distinct are the modules in the mouse mandible? Evol Dev 5:522–531.

1 Klingenberg CP, Navarro N. 2012. Development of the mouse mandible: a model system for complex
2 morphological structures. In: Macholán M, Baird SJE, Munclinger P, Piálek J, editors. Evolution of
3 the House Mouse. Cambridge: Cambridge University Press. p 135–149.

4 Mandahl N. 1992. Methods in solid tumor cytogenetics. In: Rooney DE, Czepulkowski BH, editors.
5 Human Cytogenetics. A Practical Approach. London: IRL Press. p 155–187.

6 Manning CJ, Dewsbury DA, Wakeland EK, Potts WK. 1995. Communal nesting and communal
7 nursing in house mice, *Mus musculus domesticus*. Anim Behav 50:741–751.

8 Mardia KV, Bookstein FL, Moreton IJ. 2000. Statistical assessment of bilateral symmetry of shapes.
9 Biometrika 87:285–300.

10 Martinez-Maza C, Freidline SE, Strauss A, Nieto-Diaz M. 2015. Bone growth dynamics of the facial
11 skeleton and mandible in *Gorilla gorilla* and *Pan troglodytes*. Evol Biol 43:60–80.

12 Martinez-Maza C, Montes L, Lamrous H, Ventura J, Cubo J. 2012. Postnatal histomorphogenesis of
13 the mandible in the house mouse. J Anat 220:472–483.

14 Martinez-Maza C, Rosas A, García-Vargas S. 2006. Bone paleohistology and human evolution. J
15 Anthropol Sci 84:33–52.

16 Martinez-Maza C, Rosas A, Nieto-Diaz M. 2010. Brief communication: identification of bone
17 formation and resorption surfaces by reflected light microscopy. Am J Phys Anthropol 143:313–
18 320.

19 Martinez-Maza C, Rosas A, Nieto-Diaz M. 2013. Postnatal changes in the growth dynamics of the
20 human face revealed from bone modelling patterns. J Anat 223:228–241.

21 Martínez-Vargas J, Martinez-Maza C, Muñoz-Muñoz F, Medarde N, Lamrous H, López-Fuster MJ,
22 Cubo J, Ventura J. 2017a. Comparative postnatal histomorphogenesis of the mandible in wild and
23 laboratory mice. Ann Anat 215:8–19.

24 Martínez-Vargas J, Muñoz-Muñoz F, Martinez-Maza C, Molinero A, Ventura J. 2017b. Postnatal
25 mandible growth in wild and laboratory mice: differences revealed from bone remodeling patterns
26 and geometric morphometrics. J Morphol 278:1058–1074.

27 Martínez-Vargas J, Muñoz-Muñoz F, Medarde N, López-Fuster MJ, Ventura J. 2014. Effect of
28 chromosomal reorganizations on morphological covariation of the mouse mandible: insights from a
29 Robertsonian system of *Mus musculus domesticus*. Front Zool 11:51.

30 Medarde N, López-Fuster MJ, Muñoz-Muñoz F, Ventura J. 2012. Spatio-temporal variation in the
31 structure of a chromosomal polymorphism zone in the house mouse. Heredity 109:78–89.

32 Medarde N, Martínez-Vargas J, Sánchez-Chardi A, López-Fuster MJ, Ventura J. 2013. Effect of
33 Robertsonian translocations on sperm head form in the house mouse. Biol J Linn Soc Lond
34 110:878–889.

1 Medarde N, Merico V, López-Fuster MJ, Zuccotti M, Garagna S, Ventura J. 2015. Impact of the
2 number of Robertsonian chromosomes on germ cell death in wild male house mice. Chromosome
3 Res 23:159–169.

4 Mitteroecker P, Bookstein F. 2011. Linear discrimination, ordination, and the visualization of
5 selection gradients in modern morphometrics. Evol Biol 38:100–114.

6 Mitteroecker P, Gunz P, Bernhard M, Schaefer K, Bookstein FL. 2004. Comparison of cranial
7 ontogenetic trajectories among great apes and humans. J Hum Evol 46:679–697.

8 Monteiro LR. 1999. Multivariate regression models and geometric morphometrics: the search for
9 causal factors in the analysis of shape. Syst Biol 48:192–199.

10 Muñoz-Muñoz F, Sans-Fuentes MA, López-Fuster MJ, Ventura J. 2003. Non-metric morphological
11 divergence in the western house mouse, *Mus musculus domesticus*, from the Barcelona
12 chromosomal hybrid zone. Biol J Linn Soc Lond 80:313–322.

13 Muñoz-Muñoz F, Sans-Fuentes MA, López-Fuster MJ, Ventura J. 2006. Variation in fluctuating
14 asymmetry levels across a Robertsonian polymorphic zone of the house mouse. J Zool Syst Evol
15 Res 44:236–250.

16 Muñoz-Muñoz F, Sans-Fuentes MA, López-Fuster MJ, Ventura J. 2011. Evolutionary modularity of
17 the mouse mandible: dissecting the effect of chromosomal reorganizations and isolation by
18 distance in a Robertsonian system of *Mus musculus domesticus*. J Evol Biol 24:1763–1776.

19 Navarro A, Barton NH. 2003. Chromosomal speciation and molecular divergence - accelerated
20 evolution in rearranged chromosomes. Science 300:321–324.

21 Pautke C, Vogt S, Tischer T, Wexel G, Deppe H, Milz S, Schieker M, Kolk A. 2005. Polychrome
22 labelling of bone with seven different fluorochromes: enhancing fluorochrome discrimination by
23 spectral image analysis. Bone 37:441–445.

24 Piálek J, Hauffe HC, Searle JB. 2005. Chromosomal variation in the house mouse. Biol J Linn Soc
25 Lond 84:535–563.

26 R Core Team. 2016. R: a language and environment for statistical computing. R foundation for
27 statistical computing, Vienna, Austria. http://www.R-project.org.

28 Ramirez-Yañez GO, Smid JR, Young WG, Waters MJ. 2005. Influence of growth hormone on the
29 craniofacial complex of transgenic mice. Eur J Orthod 27:494–500.

30 Renaud S, Auffray J-C, de la Porte S. 2010. Epigenetic effects on the mouse mandible: common
31 features and discrepancies in remodeling due to muscular dystrophy and response to food
32 consistency. BMC Evol Biol 10:28.

33 Rice WR. 1989. Analyzing tables of statistical tests. Evolution 43:223–225.

34 Robling AG, Castillo AB, Turner CH. 2006. Biomechanical and molecular regulation of bone
35 remodeling. Annu Rev Biomed Eng 8:455–498.

1 Robling AG, Li J, Shultz KL, Beamer WG, Turner CH. 2003. Evidence for a skeletal
2 mechanosensitivity gene on mouse chromosome 4. FASEB J 17:324–326.

3 Rohlf FJ. 2010. TpsDig2, version 2.16. Department of Ecology and Evolution, State University of
4 New York at Stony Brook. Available from URL: http://life.bio.sunysb.edu/ee/rohlf/software.html.

5 Rohlf FJ, Slice D. 1990. Extensions of the Procrustes method for the optimal superimposition of
6 landmarks. Syst Zool 39:40–59.

7 Sans-Fuentes MA, García-Valero J, Ventura J, López-Fuster MJ. 2010. Spermatogenesis in house
8 mouse in a Robertsonian polymorphism zone. Reproduction 140:569–581.

9 Sans-Fuentes MA, Muñoz-Muñoz F, Ventura J, López-Fuster MJ. 2007. Rb(7.17), a rare Robertsonian
10 fusion in wild populations of the house mouse. Genet Res 89:207–213.

11 Sans-Fuentes MA, Ventura J, López-Fuster MJ, Corti M. 2009. Morphological variation in house mice
12 from the Robertsonian polymorphism area of Barcelona. Biol J Linn Soc Lond 97:555–570.

13 Schindelin J, Arganda-Carreras I, Frise E, Kaynig V, Longair M, Pietzsch T, Preibisch S, Rueden C,
14 Saalfeld S, Schmid B, Tinevez JY, White DJ, Hartenstein V, Eliceiri K, Tomancak P, Cardona A.
15 2012. Fiji: an open-source platform for biological-image analysis. Nat Methods 9:676–682.

16 Schwarz E, Schwarz HK. 1943. The wild and commensal stocks of the house mouse, *Mus musculus*
17 Linnaeus. J Mammal 24:59–72.

18 Sjögren K, Bohlooly YM, Olsson B, Coschigano K, Törnell J, Mohan S, Isaksson OG, Baumann G,
19 Kopchick J, Ohlsson C. 2000. Disproportional skeletal growth and markedly decreased bone
20 mineral content in growth hormone receptor -/- mice. Biochem Biophys Res Commun 267:603–
21 608.

22 Starck JM, Chinsamy A. 2002. Bone microstructure and developmental plasticity in birds and other
23 dinosaurs. J Morphol 254:232–246.

24 Suzuki K, Abe S, Kim HJ, Usami A, Iwanuma O, Okubo H, Ide Y. 2007. Changes in the muscle fibre
25 properties of the mouse temporal muscle after weaning. Anat Histol Embryol 36:103–106.

26 Swiderski DL, Zelditch ML. 2013. The complex ontogenetic trajectory of mandibular shape in a
27 laboratory mouse. J Anat 223:568–580.

28 Turner CH. 1998. Three rules for bone adaptation to mechanical stimuli. Bone 23:399–407.

29 van Gaalen SM, Kruyt MC, Geuze RE, de Bruijn JD, Alblas J, Dhert WJ. 2010. Use of fluorochrome
30 labels in *in vivo* bone tissue engineering research. Tissue Eng Part B Rev 16:209–217.

31 Wallace M. 1976. Effects of stress due to deprivation and transport in different genotypes of house
32 mouse. Lab Anim 10:335–347.

33 Zelditch ML, Wood AR, Bonett RM, Swiderski DL. 2008. Modularity of the rodent mandible:
34 integrating bones, muscles, and teeth. Evol Dev 10:756–766.

1 Zelditch ML, Wood AR, Swiderski DL. 2009. Building developmental integration into functional
2 systems: function-induced integration of mandibular shape. Evol Biol 36:71–81.

3

TABLES

TABLE 1. Sample sizes for the analyses conducted in the study.

Postnatal week	St mice	Rb mice	Total
2nd	6[b]	7[b]	13[c]
3rd	7[b]	7[b]	14[c]
4th	7[b]	6[b]	13[c]
5th	6[b]	6[b]	12[c]
6th	4[b]	7[b]	11[c]
7th	3[b]	7[b]	10[c]
8th	3[b]	3[b]	6[c]
Total	36[a]	43[a]	79
2nd–4th	20[d]	20[d]	
5th–8th	16[d]	23[d]	

a, sample sizes of the two datasets grouping specimens according to their karyotype and origin, used in the geometric morphometric analyses.

b, sample sizes of the fourteen datasets (seven per each group of mice) grouping specimens of the same age within each group, used to obtain the general bone remodeling patterns and to perform geometric morphometric analyses.

c, sample sizes of the seven datasets grouping St and Rb mice according to age, created to conduct geometric morphometric analyses.

d, sample sizes of the four datasets grouping distinct age classes within each group of mice, used to test the hypothesis of modularity.

TABLE 2. Distribution of bone tissue types most frequently observed in the mandibles of St mice.

PW	n	Mandible region and subregion													
		Diastema				First molar			Second molar			Ascending ramus			
		dor	lab	ven	lin	lab	ven	lin	lab	ven	lin	C lab	C lin	V lab	V lin
2nd	**6**	w	w/pf/w	w	pf/w	w	w	w	w	w	w	w	w	w	w
3rd	**7**	w	w	w	pf/w	w	w	w	w	w	w	w	w	w	w
4th	**7**	w	w	w	pf/w	w	w	w	w	w	w	w	w	w	w
5th	**6**	w	pf/w	w	pf/w	w	w	w	w	w	w	w	w	w/pf/w	w/pf/w
6th	**4**	w	pf/w	w	pf/w	w/pf/w	w/pf/w	w	w	pf/w	w	w	w/pf/w	w/pf/w	w/pf/w
7th	**3**	w	w/pf/w	w	w	w/pf/w	w/pf/w	w	w/pf/w	w	w	w	w/pf/w	w/pf/w	w/pf/w
8th	**3**	w	w/pf/w	w	pf/w	w/pf/w	w/pf/w	w	w/pf/w	w	w	w	w/pf/w	w/pf/w	w/pf/w

Abbreviations: PW, postnatal week; n, sample size; dor, dorsal; lab, labial; ven, ventral; lin, lingual; C lab, labial area of the condylar process; C lin, lingual area of the condylar process; V lab, labial area of the ventral half; V lin, lingual area of the ventral half; w, woven bone tissue; pf, parallel-fibered bone tissue; pf/w – w/pf/w, woven and parallel-fibered bone tissues observed in that order, clockwise.

TABLE 3. Distribution of bone tissue types most frequently observed in the mandibles of Rb mice.

PW	n	Mandible region and subregion													
		Diastema				First molar			Second molar			Ascending ramus			
		dor	lab	ven	lin	lab	ven	lin	lab	ven	lin	C lab	C lin	V lab	V lin
2nd	**7**	w	w	w	w/pf/w	w	w	w	w	w	w	w	w	w	w
3rd	**7**	w	w	w	pf/w	w	w	w	w	w	w	w	w	w	w
4th	**6**	w	w	w	pf/w	w	w	w	w	w	w	w	w	w	w
5th	**6**	w	w	w	pf/w	w	w	w	w	w	w	w	w	w	w
6th	**7**	w	w/pf/w	w	pf/w	w/pf/w	w	w	w	w	w/pf/w	w/pf/w	w/pf/w	w/pf/w	w/pf/w
7th	**7**	w	w/pf/w	w	pf/w	w	w	w	w	w	w	w	w	w/pf/w	w/pf/w
8th	**3**	w	w/pf/w	w	w	w	w	w	w	w	w	w	w	w/pf/w	w/pf/w

Abbreviations: PW, postnatal week; n, sample size; dor, dorsal; lab, labial; ven, ventral; lin, lingual; C lab, labial area of the condylar process; C lin, lingual area of the condylar process; V lab, labial area of the ventral half; V lin, lingual area of the ventral half; w, woven bone tissue; pf, parallel-fibered bone tissue; pf/w – w/pf/w, woven and parallel-fibered bone tissues observed in that order, clockwise.

TABLE 4. Pattern of presence and absence of fluorescent labeling most frequently observed in the mandibles of St mice.

Mandible region	Mandible subregion[a]	Postnatal week						
		2nd	3rd	4th	5th	6th	7th	8th
Diastema	1-3							
	4-5							
	6-8							
	9-11							
	12-14							
	15-18							
First molar	1-3							
	4-5							
	6-8							
	9-11							
	12-14							
	15-17							
Second molar	1-3							
	4-5							
	6-7							
	8-10							
	11-12							
	13-14							
Ascending ramus	1-3							
	4-5							
	6-9							
	10-11							
	12-16							
	17-20							

Color legend: *white*, presence of fluorescent labeling, indicating bone deposition; *gray*, absence of fluorescent labeling, likely due to endosteal bone resorption; *black*, absence of fluorescent labeling, likely due to periosteal bone resorption; *dark blue*, absence of fluorescent labeling, likely due to dormant bone; *dark red*, absence of fluorescent labeling, unknown cause.

[a] Mandible subregions (number ranges) are set based on the localization of the points used to calculate the bone growth rates (see Figs. 4–7).

TABLE 5. Pattern of presence and absence of fluorescent labeling most frequently observed in the mandibles of Rb mice.

Mandible region	Mandible subregion[a]	Postnatal week						
		2nd	3rd	4th	5th	6th	7th	8th
Diastema	1-3							
	4-5							
	6-8							
	9-11							
	12-14							
	15-18							
First molar	1-3							
	4-5							
	6-8							
	9-11							
	12-14							
	15-17							
Second molar	1-3							
	4-5							
	6-7							
	8-10							
	11-12							
	13-14							
Ascending ramus	1-3							
	4-5							
	6-9							
	10-11							
	12-16							
	17-20							

Color legend: *white*, presence of fluorescent labeling, indicating bone deposition; *gray*, absence of fluorescent labeling, likely due to endosteal bone resorption; *black*, absence of fluorescent labeling, likely due to periosteal bone resorption; *dark blue*, absence of fluorescent labeling, likely due to dormant bone; *dark red*, absence of fluorescent labeling, unknown cause.

[a] Mandible subregions (number ranges) are set based on the localization of the points used to calculate the bone growth rates (see Figs. 4–7).

TABLE 6. Periosteal bone growth rates (mean ± standard deviation, in µm day^{-1}) of the mandibles of St and Rb mice.

PW	Mandible region and subregion[a]														
	Diastema			First molar				Second molar			Ascending ramus				
	1-5	6-11	12-18	1-5	6-8	9-11	12-17	1-5	6-10	11-14	1-3	4-9	10-11	12-16	17-20
2nd	4.6±1.6	7.3±2.1	4.2±1.4	5.0±1.3	10.0±4.3	9.5±6.6	3.6±1.3	3.8±1.4	10.3±2.1	3.1±1.2	6.4±0.0	2.3±0.6	2.6±0.0	0.9±1.2	2.0±1.8
	4.0±1.1	7.7±2.6	3.8±0.9	4.5±1.0	8.8±3.2	6.4±1.0	3.4±1.7	3.2±1.4	7.5±1.0	5.6±6.7	0.0±0.0	4.0±2.4	2.1±0.7	3.2±0.0	3.5±1.2
3rd	5.2±1.6	10.9±3.1	4.5±1.7	4.3±1.8	8.7±3.6	11.0±3.8	4.2±1.2	4.2±0.5	12.6±3.2	4.3±1.0	2.7±1.0	8.2±3.0	11.9±7.0	6.8±3.0	4.8±1.5
	4.5±0.8	7.8±1.8	4.0±1.1	4.3±0.9	7.4±2.8	7.8±3.0	3.8±0.7	4.5±1.1	9.5±2.5	3.9±1.0	2.7±2.2	8.6±3.5	4.8±2.6	5.9±2.8	4.1±1.6
4th	3.6±1.2	6.8±2.1	2.7±1.0	2.3±1.3	4.6±2.7	5.5±2.7	2.2±1.3	2.4±1.2	5.8±2.0	1.8±0.9	2.1±1.2	3.8±1.7	5.9±2.1	3.7±1.1	4.1±1.9
	3.4±2.1	6.7±3.7	2.5±1.6	3.6±2.8	4.3±2.8	7.9±4.2	2.3±1.5	2.5±1.5	6.5±3.4	2.2±1.0	3.1±2.1	4.5±1.8	4.4±1.4	4.5±2.6	4.2±1.8
5th	2.3±0.5	6.1±1.3	2.3±1.4	2.1±1.0	4.1±1.8	4.2±1.3	1.4±1.1	2.4±0.4	4.7±0.7	1.3±1.2	0.5±1.1	3.5±1.3	4.9±2.0	3.9±1.2	4.0±1.3
	2.0±0.7	5.7±1.3	2.5±1.2	1.7±0.6	3.9±1.4	4.0±1.7	2.0±1.5	2.1±1.1	4.1±1.4	1.9±1.2	2.0±1.5	2.2±0.8	4.2±1.4	3.4±1.0	4.1±0.9
6th	2.1±1.3	4.4±1.6	1.4±0.2	1.4±1.0	3.5±0.6	4.7±0.3	2.2±0.7	1.9±0.5	4.7±0.7	2.4±0.8	3.1±2.9	3.5±1.1	6.3±3.0	4.1±1.2	3.0±0.7
	1.6±0.7	3.1±0.9	1.0±0.5	1.3±1.0	3.1±0.8	3.9±0.6	1.5±0.6	1.0±0.7	4.4±0.7	1.8±1.0	3.3±2.0	2.3±0.8	3.7±2.2	3.4±1.9	4.0±0.9
7th	1.5±0.5	2.6±0.3	1.0±0.9	1.6±0.8	2.8±0.4	3.0±0.6	1.5±0.2	1.0±0.6	3.7±0.2	2.6±0.3	2.3±2.1	2.6±0.4	3.8±0.4	2.2±0.6	3.1±0.9
	1.2±0.7	3.1±0.6	1.0±0.8	1.2±0.8	2.8±0.6	3.7±0.3	1.4±0.8	1.0±0.6	3.2±0.9	1.6±1.1	1.4±1.2	2.1±1.5	2.9±1.3	2.2±1.3	2.9±1.5
8th	1.5±1.2	3.5±1.2	1.0±0.3	0.4±0.7	1.8±1.6	3.4±0.1	1.8±0.3	1.4±0.6	2.8±1.1	1.7±0.2	1.9±0.0	3.0±0.8	3.3±1.5	1.3±1.2	2.7±0.8
	0.5±0.8	1.8±0.6	0.0±0.0	0.4±0.6	1.3±1.2	2.3±1.0	1.1±0.8	0.5±0.9	1.4±2.1	0.0±0.0	0.0±0.0	1.2±1.7	1.9±1.9	0.4±0.1	0.9±1.3

For each postnatal week, upper row corresponds to St mice and lower row to Rb mice.

After applying the Mann-Whitney U test, and correcting the statistical significance with the sequential Bonferroni correction, no bone growth rate is significantly different between St and Rb mice.

Abbreviations: PW, postnatal week; n, sample size.

[a] Mandible subregions (number ranges) are set based on the localization of the points used to calculate the bone growth rates (see Figs. 4–7).

TABLE 7. Two-factor ANOVA of centroid size conducted on the whole sample.

	Centroid size				
Effect	**SS**	**df**	**MS**	**F**	***P***
Individual	68.570	71	0.966	48.73	<0.001
Side	2.807	1	2.807	141.61	<0.001
Individual × Side	1.546	78	0.020	10.50	<0.001
Age	348.829	6	58.138	60.20	<0.001
Group of mice	0.031	1	0.031	0.03	0.858
Measurement error	0.298	158	0.002		

Abbreviations: SS, sum of squares; df, degrees of freedom; MS, mean squares; F, F statistic; *P*, *P*-value.

TABLE 8. Procrustes ANOVA of shape conducted on the whole sample.

	Shape						
Effect	**SS**	**df**	**MS**	**F**	***P***	**Pillai tr**	***P***
Individual	0.323	2272	1.421×10^{-4}	5.72	<0.001	23.50	<0.001
Side	0.032	32	9.979×10^{-4}	40.15	<0.001	0.96	<0.001
Individual × Side	0.062	2496	2.485×10^{-5}	7.31	<0.001	22.17	<0.001
Age	0.216	192	1.123×10^{-3}	7.90	<0.001	3.30	<0.001
Group of mice	0.017	32	5.180×10^{-4}	3.64	<0.001	0.80	<0.001
Measurement error	0.017	5056	3.399×10^{-6}				

Abbreviations: SS, sum of squares; df, degrees of freedom; MS, mean squares; F, F statistic; *P*, *P*-value; Pillai tr, Pillai trace.

TABLE 9. Symmetric centroid size (mean ± standard deviation) of the dentary bones, and each mandible module, of St and Rb mice.

PW	Centroid size					
	Whole mandible		Alveolar region		Ascending ramus	
	St mice	Rb mice	St mice	Rb mice	St mice	Rb mice
2nd	13.80 ± 0.53	13.79 ± 0.89	6.55 ± 0.16	6.58 ± 0.26	5.00 ± 0.30	4.97 ± 0.43
3rd	15.13 ± 0.55	14.98 ± 0.38	6.94 ± 0.16	6.89 ± 0.17	5.75 ± 0.28	5.61 ± 0.17
4th	15.65 ± 0.28	15.63 ± 0.59	7.08 ± 0.20	7.02 ± 0.17	6.02 ± 0.18	6.03 ± 0.32
5th	15.93 ± 0.32	16.07 ± 0.60	7.09 ± 0.18	7.17 ± 0.17	6.21 ± 0.25	6.20 ± 0.29
6th	16.55 ± 0.24	16.93 ± 0.29	**7.17 ± 0.17***	**7.38 ± 0.12***	6.37 ± 0.19	6.49 ± 0.20
7th	16.83 ± 0.15	16.93 ± 0.33	7.22 ± 0.08	7.28 ± 0.10	6.73 ± 0.03	6.46 ± 0.22
8th	16.86 ± 0.44	16.49 ± 0.82	7.24 ± 0.17	7.12 ± 0.28	6.68 ± 0.13	6.38 ± 0.35

*, centroid sizes significantly different between the two mouse groups (P<0.05).

TABLE 10. Correlation coefficients (r) between the covariance matrices of St and Rb mice, using both raw and size-corrected data.

	r	
Postnatal week	**Raw**	**Size-corrected**
2nd	0.160*	0.256**
3rd	0.148*	0.124*
4th	0.236**	0.258**
5th	0.124*	0.164*
6th	0.223**	0.306**
7th	0.044	0.040
8th	0.513**	0.419**

*, P<0.05; **, P<0.001.

TABLE 11. Procrustes distances between St and Rb mice, using both raw and size-corrected data.

	Procrustes distances	
Postnatal week	**Raw**	**Size-corrected**
2nd	0.017	0.017
3rd	0.018	0.019
4th	0.015	0.015
5th	0.019	0.020
6th	0.036*	0.037*
7th	0.044*	0.045*
8th	0.032	0.035

*, $P<0.05$; **, $P<0.001$.

TABLE 12. Covariance ratio (CR) coefficients assessing the hypothesis of modular organization of the mandible, using both raw and size-corrected data.

	CR coefficient			
Postnatal	**St mice**		**Rb mice**	
weeks	**Raw**	**Size-corrected**	**Raw**	**Size-corrected**
2nd–4th	0.930	0.974	0.986	0.905
5th–8th	0.909*	0.853*	0.956	0.922

*, $P<0.05$.

APPENDIX

APPENDIX 1. Specimen list with information on the individual karyotypes, indicating the set and structural heterozygosity of Robertsonian translocations.

Specimen number	Age (weeks)	Sex	2n	Rb translocations[a]							Mouse group	Origin[b]
				3.8	4.14	5.15	6.10	7.17	9.11	12.13		
120511/1	2	f	29	H	M	M	M	–	M	M	Rb	CA
120511/2	2	m	29	H	M	M	M	–	M	M	Rb	CA
120611/1	2	f	31	H	M	M	–	–	M	M	Rb	CA
090601/1	2	m	32	M	M	H	–	–	M	H	Rb	LG
090605/1	2	m	32	H	M	H	H	–	H	M	Rb	LG
090630/1	2	m	34	–	H	M	–	–	M	H	Rb	CU
100608/1	2	m	36	–	M	H	–	–	–	H	Rb	SC
120518/2	3	f	29	H	M	M	M	–	M	M	Rb	CA
120518/1	3	m	29	H	M	M	M	–	M	M	Rb	CA
090615/1	3	m	29	M	M	M	M	–	H	M	Rb	LG
090608/1	3	m	31	H	H	M	H	–	M	M	Rb	LG
120618/1	3	f	32	–	M	M	–	–	M	M	Rb	CA
090708/1	3	m	33	–	H	M	–	–	M	M	Rb	CU
100615/1	3	m	37	–	H	M	–	–	–	–	Rb	SC
120525/1	4	f	29	H	M	M	M	–	M	M	Rb	CA
120625/1	4	m	30	H	M	M	H	–	M	M	Rb	CA
090615/2	4	m	32	–	M	H	H	–	M	M	Rb	LG
090622/1	4	m	32	H	M	H	H	–	H	M	Rb	LG
090714/1	4	f	35	–	–	M	–	–	M	H	Rb	CU
100622/5	4	m	36	–	M	M	–	–	–	–	Rb	SC
120601/1	5	f	29	M	M	M	H	–	M	M	Rb	CA
131031/1	5	f	31	?	H?	?	H?	?	?	?	Rb	LG
090622/2	5	m	31	–	M	M	H	–	M	M	Rb	LG
120702/1	5	m	32	–	M	M	H	–	H	M	Rb	CA
090721/2	5	f	33	–	M	M	H	–	M	–	Rb	CU
100629/1	5	f	37	–	H	H	–	–	–	H	Rb	SC
120608/1	6	m	28	M	M	M	M	–	M	M	Rb	CA
131203/1	6	f	31	?	?	?	?	?	?	?	Rb	LG
120709/1	6	m	31	–	M	M	H	–	M	M	Rb	CA
090629/2	6	m	31	H	M	M	–	–	M	M	Rb	LG
131108/1	6	m	31	?	H?	H?	H?	?	?	H?	Rb	LG
140210/2	6	m	32	H	M	M	H	–	–	M	Rb	LG
140210/1	6	f	?	?	?	?	?	?	?	?	Rb	LG

120615/1	7	m	28	M	M	M	M	–	M	M	Rb	CA
131210/3	7	f	31	H?	H?	M	?	?	M	H?	Rb	LG
131114/1	7	m	31	?	?	?	?	?	?	?	Rb	LG
131210/1	7	m	31	–	M	M	H	–	M	M	Rb	LG
131210/2	7	m	31	?	?	?	?	?	?	?	Rb	LG
140218/1	7	f	?	H?	M	?	?	?	?	M	Rb	LG
140218/2	7	f	32?	?	?	?	?	?	?	?	Rb	LG
131113/1	8	f	33	H?	H?	H?	?	?	H?	M	Rb	LG
140225/1	8	m	?	?	?	?	?	?	?	?	Rb	LG
140225/2	8	m	30?	?	H?	?	?	?	?	H?	Rb	LG
100318/1	2	f	40	–	–	–	–	–	–	–	St	CB
120618/2	2	f	40	–	–	–	–	–	–	–	St	CB
120803/8	2	f	40	–	–	–	–	–	–	–	St	CB
090603/1	2	m	40	–	–	–	–	–	–	–	St	CV
120803/7	2	m	40	–	–	–	–	–	–	–	St	CB
110411/2	2	m	40	–	–	–	–	–	–	–	St	SP
120810/2	3	f	40	–	–	–	–	–	–	–	St	CB
120810/1	3	f	40	–	–	–	–	–	–	–	St	CB
091202/1	3	f	40	–	–	–	–	–	–	–	St	NU
090610/2	3	m	40	–	–	–	–	–	–	–	St	CV
100325/1	3	m	40	–	–	–	–	–	–	–	St	CB
120625/2	3	m	40	–	–	–	–	–	–	–	St	CB
090602/1	3	m	40	–	–	–	–	–	–	–	St	SP
090617/1	4	f	40	–	–	–	–	–	–	–	St	CV
120702/2	4	f	40	–	–	–	–	–	–	–	St	CB
120817/2	4	f	40	–	–	–	–	–	–	–	St	CB
120817/1	4	f	40	–	–	–	–	–	–	–	St	CB
100401/1	4	m	40	–	–	–	–	–	–	–	St	CB
091209/1	4	m	40	–	–	–	–	–	–	–	St	NU
090609/1	4	m	40	–	–	–	–	–	–	–	St	SP
120709/2	5	f	40	–	–	–	–	–	–	–	St	CB
091216/1	5	f	40	–	–	–	–	–	–	–	St	NU
090625/1	5	m	40	–	–	–	–	–	–	–	St	CV
100408/1	5	m	40	–	–	–	–	–	–	–	St	CB
120824/1	5	m	40	–	–	–	–	–	–	–	St	CB
090612/1	5	m	40	–	–	–	–	–	–	–	St	SP
150119/1	6	f	40	–	–	–	–	–	–	–	St	CV
150119/3	6	f	40	–	–	–	–	–	–	–	St	CV
150119/2	6	m	40	–	–	–	–	–	–	–	St	CV
091223/1	6	m	40	–	–	–	–	–	–	–	St	NU

150126/2	7	f	40	–	–	–	–	–	–	–	St	CV
150126/3	7	f	40	–	–	–	–	–	–	–	St	CV
150126/1	7	m	40	–	–	–	–	–	–	–	St	CV
150109/3	8	f	40	–	–	–	–	–	–	–	St	CV
150109/1	8	m	40	–	–	–	–	–	–	–	St	CV
150109/2	8	m	40	–	–	–	–	–	–	–	St	CV

[a] Pairs of numbers below *Rb translocations* indicate the pairs of acrocentric chromosomes involved in the Rb translocation (*a* and *b*) and thus in the formation of the resulting metacentric chromosome (*a.b*).

[b] *Origin* refers to the collection sites of the biological mothers.

Abbreviations: f, female; m, male; 2n, diploid number; M, homozygous metacentric (two copies of the metacentric indicated, each resulting from the fusion of the same two non-homologous acrocentrics, are identified); H, heterozygous metacentric (two non-homologous acrocentrics are fused forming a metacentric, while their respective homologues are found as acrocentrics); –, absent metacentric (the metacentric indicated is not detected; instead, the two non-homologous chromosomes are present as acrocentrics); ?, non-identified metacentric (the karyotyping failed, which impeded the identification of chromosomes); Rb, individual with Rb translocations, with a diploid number inferior to 2n=40; St, individual with the standard karyotype of 2n=40 chromosomes, without Rb translocations; CA, Castelldefels; CB, Castellfollit del Boix; CU, Cubelles; CV, Castellar del Vallès; LG, La Granada; NU, Nulles; SC, Santa Coloma de Queralt; SP, Santa Perpètua de Mogoda.

FIGURE LEGENDS

Fig. 1. Lingual view of a right dentary bone, with the layout of the landmarks used in the geometric morphometric analyses (numbers), and the localization of the histological cross-sections: (**A**) diastema region; (**B**) first molar region; (**C**) second molar region; (**D**) ascending ramus region at the level of the condylar and angular processes. The dashed line subdivides the landmarks according to the hypothesis of modularity. Scale bar: 5mm.

Fig. 2. Histological cross-sections of a mandible of *Mus musculus domesticus* under natural light: (**A**) diastema region; (**B**) first molar region; (**C**) second molar region; (**D**) ascending ramus region at the level of the condylar and angular processes. Scale bar: 1mm.

Fig. 3. Types of bone tissue identified in the histological cross-sections of the mandible of *Mus musculus domesticus* under natural light: (**A**) woven bone tissue; (**B**) parallel-fibered bone tissue. Scale bars: 100µm.

Fig. 4. Histological cross-section of the diastema region under ultraviolet light with the measurement points (left), and ontogenetic patterns of periosteal bone growth rate (mean ± standard deviation, in µm day^{-1}) of its subregions (right): (**A**) dorsal area, and dorsal half of the labial area (points 1-5); (**B**) ventral half of the labial area, and ventral area (points 6-11); (**C**) lingual area (points 12-18). Scale bar: 1mm. Abbreviation: BGR, bone growth rate. See Table 6 for numerical values.

Fig. 5. Histological cross-section of the first molar region under ultraviolet light with the measurement points (left), and ontogenetic patterns of periosteal bone growth rate (mean ± standard deviation, in µm day^{-1}) of its subregions (right): (**A**) dorsal half of the labial portion (points 1-5); (**B**) ventral half of the labial area (points 6-8); (**C**) ventral area (points 9-11); (**D**) lingual area (points 12-17). Scale bar: 1mm. Abbreviation: BGR, bone growth rate. See Table 6 for numerical values.

Fig. 6. Histological cross-section of the second molar region under ultraviolet light with the measurement points (left), and ontogenetic patterns of periosteal bone growth rate (mean ± standard deviation, in μm day^{-1}) of its subregions (right): (**A**) labial area (points 1-5); (**B**) ventral area (points 6-10); (**C**) lingual area (points 11-14). Scale bar: 1mm. Abbreviation: BGR, bone growth rate. See Table 6 for numerical values.

Fig. 7. Histological cross-section of the ascending ramus region at the level of the condylar and angular processes under ultraviolet light with the measurement points (left), and ontogenetic patterns of periosteal bone growth rate (mean ± standard deviation, in μm day^{-1}) of its subregions (right): (**A**) labial area of the condylar process (points 1-3); (**B**) labial area of the ventral half (points 4-9); (**C**) ventral area of the angular process (points 10-11); (**D**) lingual area of the ventral half (points 12-16); (**E**) lingual area of the condylar process (points 17-20). Scale bar: 1mm. Abbreviation: BGR, bone growth rate. See Table 6 for numerical values.

Fig. 8. Fields of bone deposition (**A**) and bone resorption (**B**). Scale bars: 100μm.

Fig. 9. Bone remodeling patterns of the labial (**A**) and lingual (**B**) surfaces of the left dentary bone of Rb and St mice, most frequently observed in each postnatal week. *Light grey areas* represent bone deposition fields; *dark grey areas* represent bone resorption fields; *white areas* correspond to bone surfaces with no histological data. Abbreviation: PW, postnatal week.

Fig. 10. Symmetric centroid size (mean ± standard deviation) of the mandible in St and Rb mice over ontogeny. Abbreviation: CS, centroid size.

Fig. 11. Diagrams of allometric shape changes (eigenvectors) in each mouse group over ontogeny, corresponding to an increase in centroid size of 4.0 units.

Fig. 12. (**A**) Scatter plot of between-group PC1 versus PC2 raw scores according to age and group. Abbreviations: PW, postnatal week; PC1, first between-group principal component; PC2, second between-group principal component. PC1 axis has been flipped so that older animals appear to the right, following the common convention. (**B**) Diagrams of shape changes (eigenvectors) along PC1 and PC2 axes. Scale factor: 0.1 units in positive direction from the consensus (outline and center of coordinates).

Fig. 13. Scatter plot of PC1 versus PC2 scores in size-shape space. Abbreviations: PW, postnatal week; PC1, first principal component; PC2, second principal component.

Fig. 14. Ontogenetic trajectories, displayed as lines, projected onto the first two principal components of between-group shape variation. White circles represent the mean of the 2nd postnatal week, black circles represent the mean of the 8th postnatal week, and grey circles represent the mean of the intermediate age stages. Abbreviations: PC1, first between-group principal component; PC2, second between-group principal component.

Figure 1

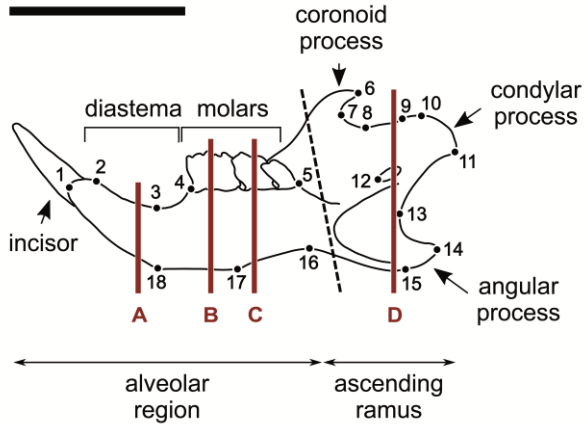

Figure 2

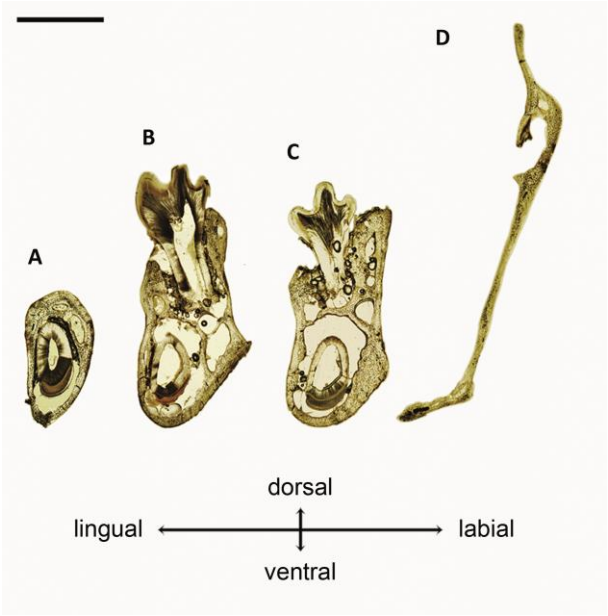

Figure 3

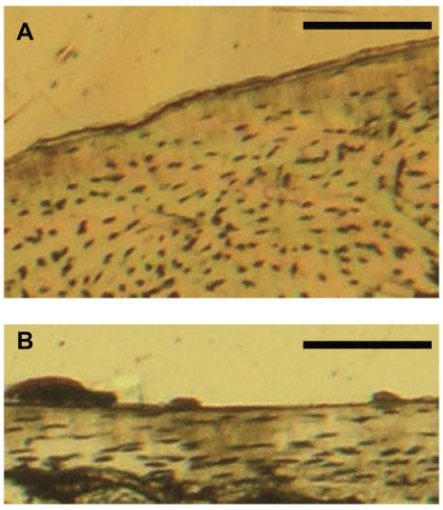

Figure 4

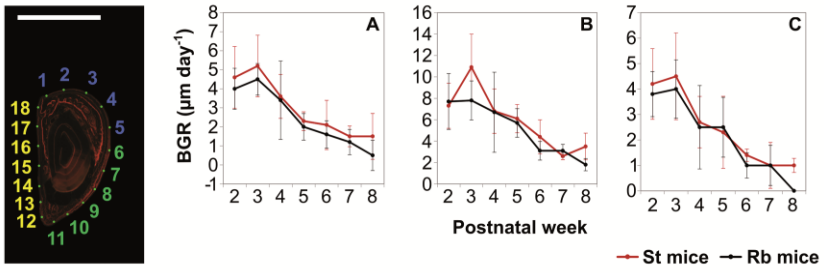

Figure 5

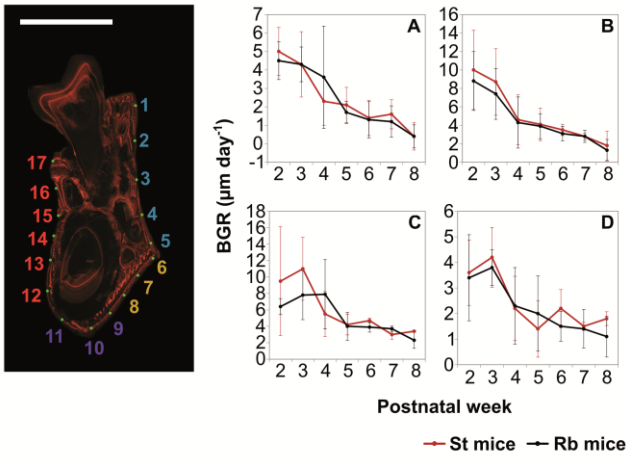

Figure 6

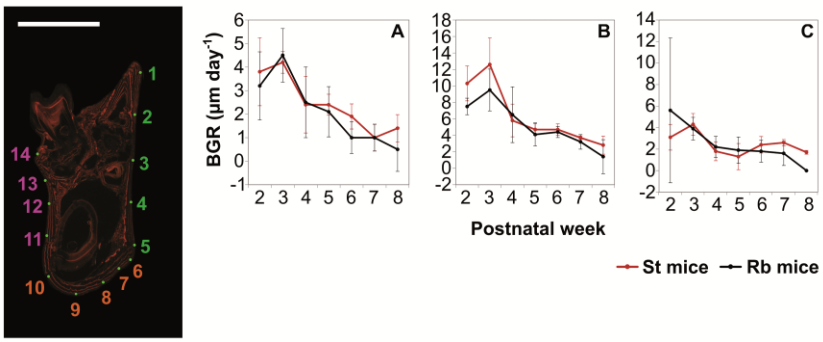

Figure 7

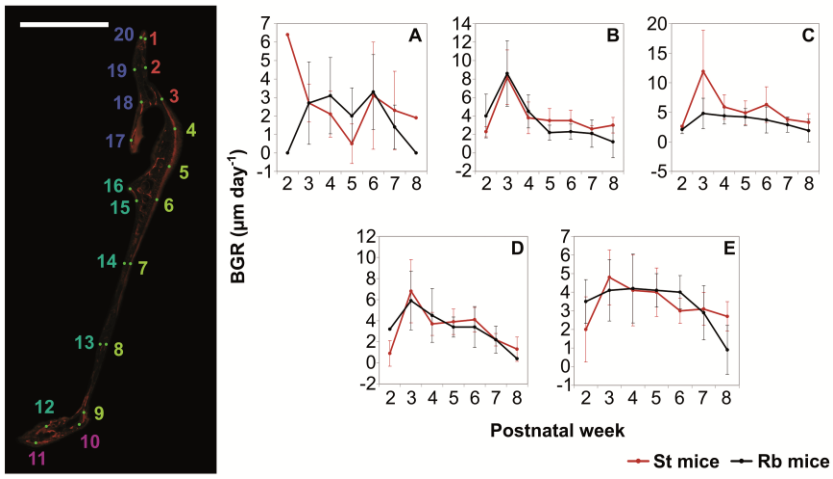

Figure 8

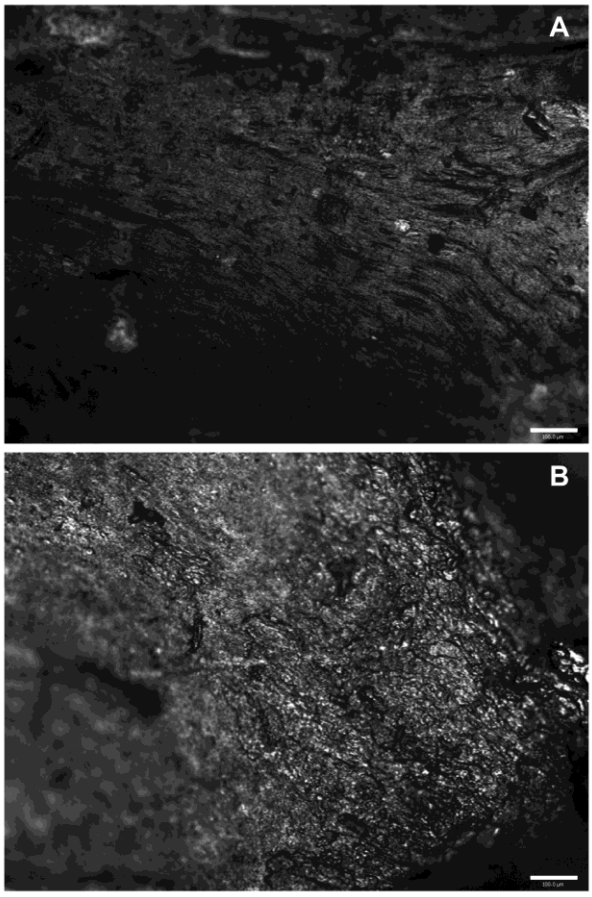

Figure 9

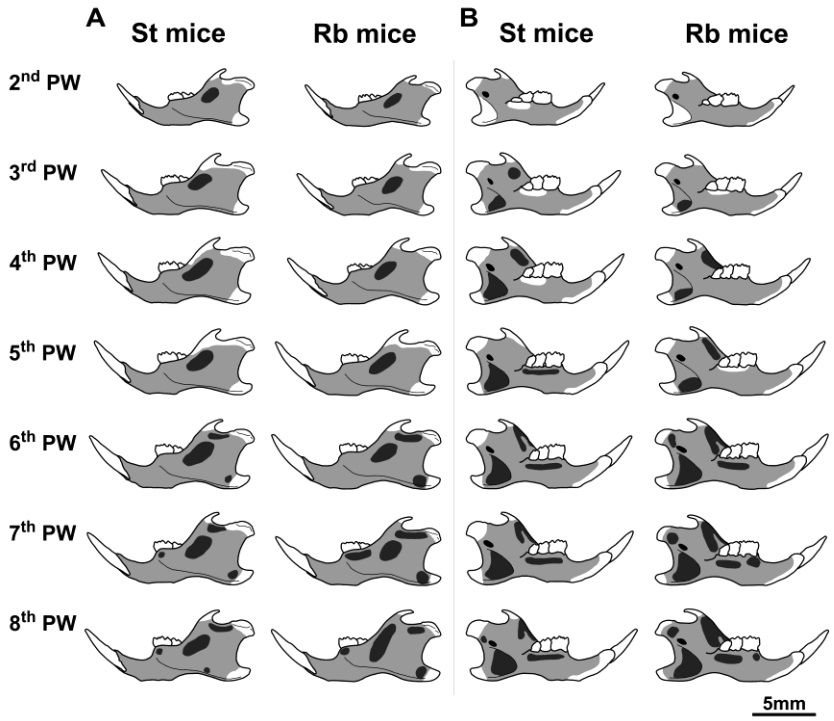

Figure 10

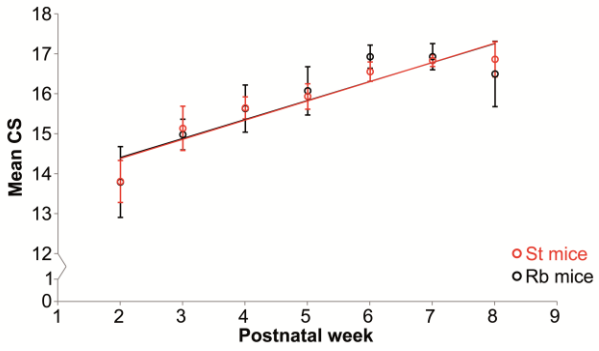

Figure 11

Figure 12

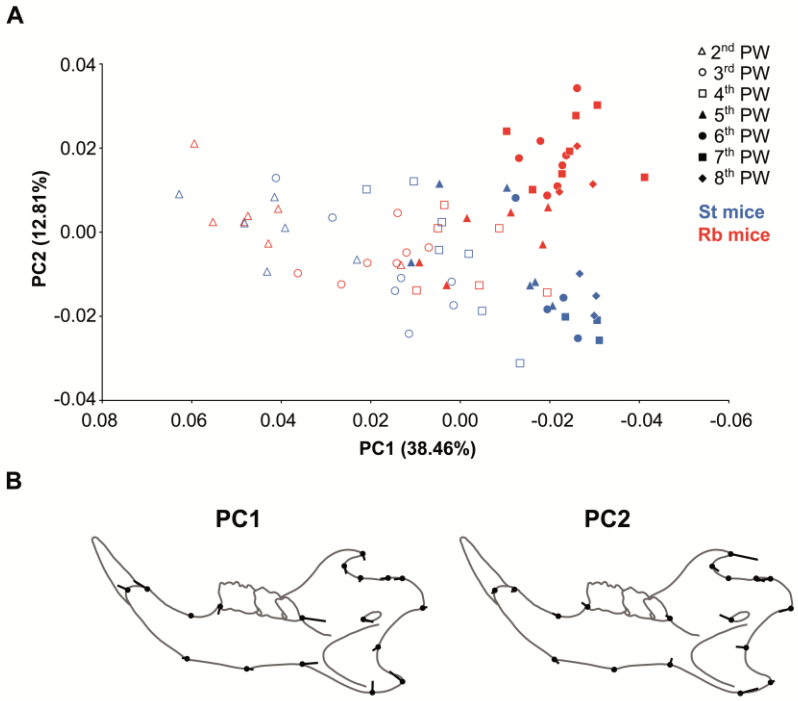

Figure 13

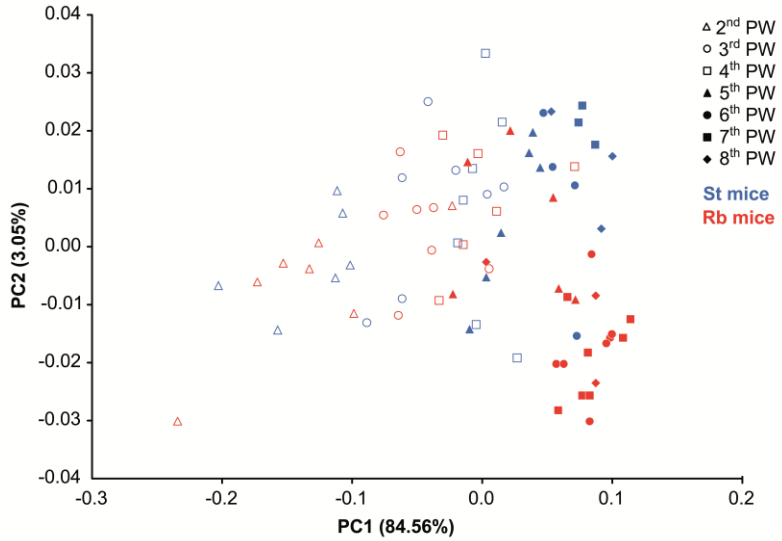

Figure 14